ISTANBUL TECHNICAL UNIVERSITY ★ GRADUATE SCHOOL

MECHANICAL PROPERTIES OF BORON NANOTUBES

M.Sc. THESIS

Erdem ÇALIŞKAN

Department of Mechanical Engineering

Solid Mechanics Program

November 2021

ISTANBUL TECHNICAL UNIVERSITY ★ GRADUATE SCHOOL

MECHANICAL PROPERTIES OF BORON NANOTUBES

M.Sc. THESIS

Erdem ÇALIŞKAN
503191531

Department of Mechanical Engineering

Solid Mechanics Program

Thesis Advisor: Assoc. Prof. Dr. Mesut KIRCA

November 2021

ISTANBUL TEKNİK ÜNİVERSİTESİ ★ LİSANSÜSTÜ EĞİTİM ENSTİTÜSÜ

BOR NANOTÜPLERİN MEKANİK ÖZELLİKLERİ

YÜKSEK LİSANS TEZİ

Erdem ÇALIŞKAN
503191531

Makina Mühendisliği Anabilim Dalı

Katı Cisimlerin Mekaniği Programı

Tez Danışmanı: Doç. Dr. Mesut KIRCA

Kasım 2021

Erdem Çalışkan, a M.Sc. student of ITU Graduate School student ID 503191531 successfully defended the thesis entitled "MECHANICAL PROPERTIES OF BORON NANOTUBES", which he prepared after fulfilling the requirements specified in the associated legislations, before the jury whose signatures are below.

Thesis Advisor :	**Assoc. Prof. Dr. Mesut KIRCA** Istanbul Technical University	.....
Jury Members :	**Prof. Dr. Alp Er KONUKMAN** Gebze Technical University	.....
	Assoc. Prof. Dr. Atakan ALTINKAYNAK Istanbul Technical University	.....

Date of Submission : 15 October 2021
Date of Defense : 05 November 2021

To my family and friends,

FOREWORD

This thesis wouldn't be possible without the support and dedication of my advisor, Assoc. Prof. Dr. Mesut Kırca. I was fortunate to work with him in my undergraduate to carry on with my research to master's degree. I am grateful for his encouragement and vision, which have guided me to build my character and profession. His engagement with students in research and teaching has been and will be an inspiration for many.

I am indebted to of my family, for their unconditional love and support throughout my life. It wouldn't be possible for me to achieve any success without their contributions.

I would like to thank my genuine group of friends, Emre, Ender, İzzet, and Tarık for standing with me since I was a freshman in ITU. Their impact substantially helped me to become the person I want to be. Moreover, thanks to them, the hardship of the pandemic was endurable despite the distances. Likewise, I am thankful for the friendship of Oğulcan and Ersin, all of whom I've met on the Facilis Vehicle Team. I feel privileged to work with them as I took my first steps towards engineering.

I would also like to thank my dear friends Enes Kamil, Esra, Murathan, and Ebru, whose absence can't be filled. I'm also lucky to have a such close friend and roommate, Enes. I wish them all the best in their future. I acknowledge many wonderful friends whom names aren't here that I am grateful for their support.

Computing resources used in this work were partially provided by the National Center for High Performance Computing of Turkey (UHeM, grant numbers 1010562021 and 4010542021) and TUBITAK ULAKBIM, High Performance and Grid Computing Center (TRUBA).

November 2021

Erdem ÇALIŞKAN
Mechanical Engineer

TABLE OF CONTENTS

Page

ABBREVIATIONS

AIREBO : Adaptive Intermolecular Reactive Empirical Bond Order
BNNT : Boron-Nitrate Nanotube
BNT : Boron Nanotube
BO : Bond Order
CG : Conjugate-Gradient
CNT : Carbon Nanotube
CUDA : Compute Unified Device Architecture
DFT : Density Functional Theory
EAM : Embedded-Atom Method
HPC : High-Performance Computing
LAMMPS : Large-Scale Atomic/Molecular Massively Parallel Simulator
LDA : Local Density Approximation
LJ : Lennard-Jones
MD : Molecular Dynamics
MEAM : Modified Embedded-Atom Method
MPI : Message Passing Interface
MSM : Molecular Structural Mechanics
OMP : OpenMP multi-threading
PE : Potential Energy
ReaxFF : Reactive Force Field
REBO : Reactive Empirical Bond Order
SW : Stillinger-Weber
TEM : Transmission Electron Microscopy
vdW : van-der-Waals

SYMBOLS

E	**:** Young's modulus
p	**:** Momentum
q	**:** Charge of an atom
r	**:** Position of atoms
t	**:** Thickness
U	**:** Potential energy
δt	**:** Timestep
ϵ	**:** Dielectric constant
η	**:** Vacancy ratio
σ	**:** Stress
σ_0^{ut}	**:** Ultimate tensile stress of the non-porous nanotube
σ^{ut}	**:** Ultimate tensile stress

LIST OF TABLES

Page

LIST OF FIGURES

Page

MECHANICAL PROPERTIES OF BORON NANOTUBES

SUMMARY

Boron nanotubes (BNTs) which can be considered as structural analogs of carbon nanotubes (CNTs) and boron nitride nanotubes (BNNTs) offer remarkable mechanical, electrical, and chemical properties. As the building unit of BNTs, boron, the fifth element in the periodic table, is the lightest elemental substance that can form interatomic covalent bonds possessing multiple bonding states, which in turn provides a variety of allotropes with diverse physical and chemical properties. BNTs exhibit metallic behavior regardless of their chirality and diameters, which renders them extremely attractive in the design of novel electronic nanodevices, such as field-effect transistors, light-emitting diodes, field emission displays. In these applications, mechanical properties play a significant role since the mechanical strain is usually employed to adjust the electronic properties of the BNTs. Therefore, mechanical properties, such as tensile strength and elastic Young's modulus, of the boron nanotube structures hold significant importance.

In literature, most of the theoretical studies regarding the boron nanotubes are based on the first-principles density functional theory calculations. As an alternative approach, reactive molecular dynamics can provide accurate and quick results depending on the accuracy of the force field. Furthermore, unlike density functional theory calculations, molecular dynamics can be used to investigate large systems. In the present study, boron nanotubes are simulated using reactive molecular dynamics simulations. Although this method has been extensively practiced for borophene, to the best of our knowledge, it has not been used to simulate BNTs yet.

We created 10 different BNTs with different vacancy ratios ranging between 0 and 0.33 in two different chiral directions, zigzag and armchair. Simulations are conducted for different diameters, lengths, and aspect ratios using four different strain rates and three different temperatures, 1, 300, and 600 K. We conducted tensile tests to inspect the mechanical properties.

Mechanical properties and thermal stabilities of BNTs are highly dependent on their vacancy ratio, atomic configuration, and chirality. Our results indicate that BNTs with exhibit highly anisotropic behavior. Young moduli and ultimate tensile stress of nanotubes are generally two times higher in the zigzag direction, yet the ultimate tensile strain is two times higher in the armchair direction, except for some configurations. Stiffness and strength in general decrease while the vacancy ratio and temperature increase. The potential energy difference per atom due to the bond order is the main root of the defect formation. Some structures exhibit plastic behavior owing to stable bond formations during tensile.

We believe that our study will drive further research for BNTs using classical molecular dynamics since it will allow large-scale simulation and modeling. Their vacancies can be exploited for several applications such as hydrogen storage. Thermal properties, nanocomposites with BNTs can be subject to future studies.

BOR NANOTÜPLERİN MEKANİK ÖZELLİKLERİ

ÖZET

Karbon nanotüpler (KNT) ve bor nitrat nanotüpler (BNNT) ile yapısal benzerlikler gösteren bor nanotüpler (BNT); üstün mekanik, elektriksel ve kimyasal özelliklerinden dolayı araştırmacıların ilgisini çeken nano malzemelerdir. Bor nanotüplerin yapı taşı, periyodik tablodaki beşinci element olan bor, atomları arasında farklı tiplerde kovalent bağlar kurabilen en hafif atomdur. Bu sayede fiziksel ve kimyasal özellikleri farklı olan allotroplar oluşturabilmektedir. Bor nanotüpler, karbon nanotüplerden farklı olarak, yarıçaplarından ve heliselliklerinden bağımsız olarak metalik özellik göstermektedir. Bu durum bor nanotüpleri nano elektronik cihazların tasarımında kullanışlı kılmaktadır. Aynı zamanda, bu uygulamalarda mekanik birim uzama ile elektronik özelliklerin kontrolü yapıldığından çekme dayanımı ve elastik Young modülü gibi mekanik özellikler detaylı olarak incelenmelidir.

Yapısal kararlılığa sahip bor nanotüpler ilk olarak 1997 yılında Boustani ve Quandt tarafından önerilmiştir. İlk prensip hesaplamaları kullanarak yaptıkları çalışmalarında bor nanotüplerin ve borofen tabakaların yapısal ve elektronik özelliklerini incelemiş ve bor atomlarının birkaç farklı tipte allotropik yapılar ve bor nanotüpler oluşturabildiklerini bulmuşlardır. Bu çalışmayı takiben Ciuparu vd. 2004 yılında Mg-MCM-41 katalist üzerinde ilk defa saf bor nanotüp sentezi gerçekleştirmiştir. 2004 yılından günümüze devam edilen deneysel çalışmalarda farklı yöntemler kullanılarak da bor nanotüp allotropları sentezlenmesi başarılmıştır.

Bor nanotüpler birim hücrelerindeki boşluk sayısının toplam atom yeri sayısına oranına göre isimlendirilmektedir. Literatürde boşluk oranı η ile gösterilmektedir. Aynı boşluk oranlarında faklı hücre yapısı olabileceğinden allotroplara genellikle özel isimler verilmiştir. Bu çalışmada 2-pmmn (η=0, kısmi düzlemsel üçgen kafes yapılı), β_{12} ve β_{13} (η=1/6), β_4 (η=1/8), β_5 (η=2/15), χ_3 (η=1/5), α (η=1/9), δ_3 (η=1/3), $\eta_{1/8b}$ ve $\eta_{4/27}$ yapıları incelenmiştir.

Literatürde çapı 1,7 nanometre (nm) veya 2 nm'den düşük α-BNT'lerin bazı atomlarının eğrileşme kaynaklı düzlem dışı burkulmasından dolayı Fermi seviyesinde oluşan bant açılması sebebiyle yarı iletken özellik gösterebileceğini iddia eden çalışmalar bulunmaktadır. Ancak, takip eden çalışmalarda yüzey burkulmasının standart yoğunluk fonksiyonel teorisinden kaynaklı yapay bir olgu olduğu gösterilmiştir. Bu çalışmalar, hesaplamalı olarak Møller–Plesset pertübasyon teorisi ve dağılım-düzeltimli yoğunluk fonksiyonel teorisine ve deneysel çalışmalara dayanmaktadır. Dolayısıyla, araştırmacılar yüzey burkulması olmayan durumlarda α-BNT'lerin tamamen metalik olduğu sonucuna ulaşmıştır. Literatürde çeşitli bor nanotüp allotroplarının; çaptan, kafes yapısından ve kirallikten bağımsız olarak metalik özellik gösterdiğini belirten çalışmalar mevcuttur. Bor nanotüpleri tam metalik özelliğinden dolayı, alan etkili transistörler, ışık yayıcı diyotlar, alan emisyonlu ekranlar gibi yeni elektronik nano malzemelerin tasarımında oldukça avantajlıdır. Aynı zamanda, mekanik birim uzama elektronik özelliklerin kontrolü için

kullanıldığından; elastisite modülü, kopma dayanımı ve kopma birim uzaması gibi mekanik özellikler bu tür uygulamalarda önemli bir rol oynamaktadır.

Nano seviyede yapılan deneysel çalışmaların belirsizlikler barındırmasının yanı sıra, karmaşık ve pahalı olduğu bilinmektedir. Bu durum sayısal simülasyon tekniklerini alternatif olarak öne çıkarmaktadır. BNT'lerin mekanik özelliklerinin incelenmesi için günümüze kadar genellikle yoğunluk fonksiyonel teorisi tabanlı kuantum mekaniği hesaplamaları kullanılmıştır. Nano malzemelerin fiziksel ve kimyasal özelliklerinin incelenmesinde kullanılan bir diğer yöntem moleküler dinamik simülasyonlarıdır. Bu yöntem, kullanılan potansiyele bağlı olarak güvenilir sonuçlar vermektedir. Aynı zamanda hızlı ve çok sayıda parçacığın aynı anda modellenebilmesine olanak sağlamaktadır. Dolayısıyla, moleküler dinamik simülasyonları sıklıkla tercih edilen atomik simülasyon tekniklerinden biridir. Yapılan çalışmada bor nanotüpler reaktif moleküler dinamik simülasyon yöntemi ile modellenmiştir. BNT'lerin iki boyutlu formu olan borofenler için sıklıkla kullanılan bu yöntem, araştırmacının bilgisi dâhilinde, bor nanotüpler için ilk defa uygulanmıştır.

Moleküler dinamik simülasyonlarında atomlar arasındaki etkileşimi modellemek için Adri van Duin vd. tarafından geliştirilen ReaxFF olarak bilinen reaktif kuvvet alanı (potansiyel fonksiyonu) kullanılmıştır. Bu kuvvet alanı sürekli olarak bağ oluşumuna ve kırılmasına izin vermektedir. Bor atomları arasındaki ReaxFF parametreleri için Pai vd. tarafından sıvı karbon-bor-nitrojen malzemelerin modellenmesi için hesaplanan $ReaxFF_{CBN}$ parametrizasyonu kullanılmıştır. Bu potansiyelin iki boyutlu borofen için ilk prensip hesaplamalarına yakın sonuç verdiği bulunmuştur. Literatürde bor tabanlı malzemelerin simülasyonu için, Stillinger-Weber, Tersoff gibi, farklı potansiyeller bulunsa da, bu potansiyel fonksiyonları ile sadece belirli konfigürasyonlar modellenebilmektedir. Yazarın bilgisi dâhilinde ReaxFF dışında tüm bor nanotüp konfigürasyonlarının modellenmesine olanak sağlayan başka bir potansiyel fonksiyonu bulunmamaktadır.

Bor nanotüp yapıların elde edilmesi için ideal kafes yapısına sahip borofenleri oluşturan ve istenen eksende çevirerek bor nanotüp haline getiren kodlar oluşturulmuştur. Birim hücre parametreleri kısmi düzlemsel yapılar için a, b ve h doğrultularında sırasıyla 1.614, 2.866 ve 0.911 Å; düzlemsel yapılar için a ve b doğrultularında sırasıyla 2.926 ve 5.608 Å olarak alınmıştır.

Moleküler dinamik simülasyonları açık kaynak kodlu Large-scale Atomic/Molecular Massively Parallel Simulator (LAMMPS) programı ile yapılmıştır. Zaman integrasyonu için Hız Verlet (Velocity Verlet) adı verilen algoritma kullanılmıştır. LAMMPS içerisinde Aktulga vd. tarafından uygulanan ReaxFF ve ReaxC-OMP paketleri kullanılmıştır. Eksen doğrultusunda sınır etkisinin kaldırılması için periyodik sınır koşulu uygulanmıştır. Diğer doğrultularda 50 Å vakum boşluğu bırakılmıştır. Kodlar ile elde edilen ideal yapılara konjuge-gradyan metodu ile enerji minimizasyonu yapılmıştır. Daha sonra yapılar 1 ps boyunca Nose´-Hoover barostatı ve termostatı kullanan NPT istatistiksel kümesi ile sıfır gerilme durumuna getirilmiştir. Yapılara çekme testi sırasında $1x10^9$, $1x10^{10}$ ve $1x10^{11}$ 1/s hızında sabit mühendislik birim uzaması uygulanmıştır. Tek eksenli çekme sırasında diğer eksenlerdeki gerilmenin sıfırda tutulması için NPT istatistiksel kümesi kullanılmıştır. Makroskobik gerilme tensörü sanal gerilme teoremi kullanılarak hesaplanmıştır. Literatürde bor filmlerinin kalınlığı için mutabık bir sonuç bulunmadığından sonuçlar kalınlıktan bağımsız verilmiştir. Kalınlık belirlendiği durumda bu çalışmada verilen sonuçlar kalınlığa bölünerek gerilme birimi (GPa) cinsinden elde edilebilir.

Sonuçlara göre ReaxFF potansiyel alanının başarı ile enerji minimizasyonu yapabildiği görülmüştür. ReaxFF ile simülasyonu yapılan nanotüplerin, 1,61 nm çapında merdiven doğrultusunda δ_3 yapısı hariç, izotermal-izobarik istatistiksel küme ile termal kararlıklarını koruyabildiği görülmüştür. Çalışmamızda, Mortazavi ve diğerlerinin borofen için bulduğu sonuçlara benzer olarak, enerji minimizasyonu ve termalizasyon sırasında birim hücre parametrelerinin değiştiği görülmüştür. Enerji minimizasyonu sırasında simülasyon kutusunun boyutları eksenel ve tercih edilen radyal doğrultuda sırasıyla yaklaşık %10 ve %20 artmaktadır. Yoğunluk fonksiyonel teorisine göre birim hücre parametreleri farklı olsa da mekanik cevabın yakın sonuç verdiği gözlemlenmiştir.

Bor nanotüplerin Fermi seviyesindeki bantlarından dolayı tercih edilen doğrultuda radyal yönde genişlemesi, kuantum mekaniği temelli yoğunluk fonksiyonel teorisi hesaplamalarında gözlemlenmiştir. Bu durum nanotüpün elips şeklini almasına sebep olmaktadır. Benzer şekilde, gerçekleştirilen reaktif moleküler dinamik simülasyonlarında enerji minimizasyonu ve termalizasyon sırasında dairesel yapının elipse dönüştüğü görülmüştür. Ayrıca literatürde çeşitli kuantum mekaniği seviyesindeki çalışmalarda gözlemlenen, altıgen hücrelerin ortasında bulunan atomların yüzey burkulması, gerçekleştirdiğimiz reaktif moleküler simülasyonlarında da gözlemlenmiştir. Bu benzerlikler, ReaxFF potansiyel fonksiyonunun bor nanotüplerin yapısal özelliklerini modelleme kapasitesine sahip olduğuna işaret eden göstergelerdir.

Üçgen kafes yapılı bor nanotüpün zigzag doğrultusunda karbon nanotüplerden daha yüksek kopma dayanımına ve elastisite modülüne sahip olduğu görülmüştür. Genel olarak bor nanotüplerde gevrek kırılma gerçekleşmektedir. χ_3 merdiven, α merdiven, ve α zigzag yapıları sırasıyla en yüksek kopma dayanımı, kopma birim uzaması ve Young modülüne sahip yapılardır. Kopma dayanımı genellikle sıcaklık ve boşluk oranı arttıkça düşmektedir.

Termal ve yapısal kararlılığa sahip bor nanotüpler karbon nanotüp veya bor-nitrat nanotüp gibi yapıların yerini alabilecek özelliklere sahiptir. Metalik yapıları ile elektronik nano yapıların yapıtaşı olabilme kapasiteleri bulunmaktadır. Ek olarak, doğal yapılarında bulunan boşluklar sayesinde hidrojen gibi çeşitli malzemelerin depolamasında kullanılabilir. Yapı içerisindeki boşluklar diğer atom veya moleküller için bağ noktası görevi görmektedir. Geliştirdiğimiz yöntem bor nanotüplerin termal özelliklerinin incelenmesi veya çeşitli nano kompozit yapılarda davranışlarının incelenmesinde kullanılabilir.

1. INTRODUCTION

The discovery of carbon nanotubes (CNTs) [1] and subsequently the synthesis of graphene [2] sparked a great doping effect for the subsequent research studies on low-dimensional materials. In addition to experimental studies trying to synthesize new low-dimensional nanomaterials, many researchers also presented theoretical studies with the aim of exploiting alternative materials [3]. In recent years, new two-dimensional nanomaterials including silicane [4,5], germanene [6,7], and borophene [8,9], which can be considered as the counterparts of graphene with the base elements of silicon, germanium, and boron, respectively, have been successfully synthesized. Owing to their extraordinary mechanical, electrical, and chemical properties, these low-dimensional materials attract significant attention from the scientific community.

1.1 Borophene and Boron Nanotubes

Among recently-developed mono-layered nanomaterials, borophene presents remarkable properties due to the chemical and structural complexity of the fascinating element boron. Boron, the fifth element in the periodic table, is the lightest elemental substance that can form interatomic covalent bonds possessing multiple bonding states, which in turn provides formations of a variety of allotropes with diverse physical and chemical properties [10–12].

In low dimensional materials science, the synthesis of two-dimensional boron films, namely borophene, can be considered as crucial progress [3,8,9]. Similar to the carbon allotropes such as graphene, CNTs, and fullerenes, boron allotropes including borophene and boron nanotubes (BNTs) gather significant attention in the scientific community due to their notable properties such as low density, outstanding chemical stability, high mechanical strength, and high melting point [13]. Among different allotropic forms of boron, BNTs with structural stability are firstly proposed by Boustani and A. Quandt in 1997 [14]. In their computational study, they predicted structural and electronic properties of BNTs and boron sheets using ab initio methods and concluded that the boron atoms can form several different types of allotropic

structures as well as boron nanotubes. An illustration of their findings is given in Figure 1.1 : .

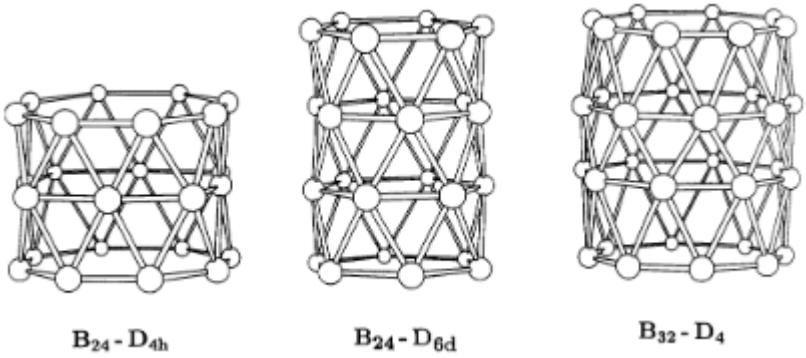

Figure 1.1 : Tubular stable boron clusters predicted by Boustani and A. Quandt in 1997 [14].

Following the computational study presenting the existence of thermodynamically feasible BNT structures in 1997, Ciuparu et al. [15] successfully synthesized pure BNT structure on Mg-MCM-41 catalyst for the first time in 2004. Their transmission electron microscopy (TEM) in Since then there have been several other studies concerning the synthesis of BNTs. For instance, Liu et al. [16] accomplished fabricating single-walled BNTs with diameters between around 10 to 40 nm using a thermal evaporation method and studied their electric transport and field emission properties, showing that individual BNTs can sustain high current densities. Furthermore, Liu and Iqbal [17] managed to synthesize single-walled BNTs with a diameter of around 20 nm and double-walled BNTs with a diameter of around 10 nm.

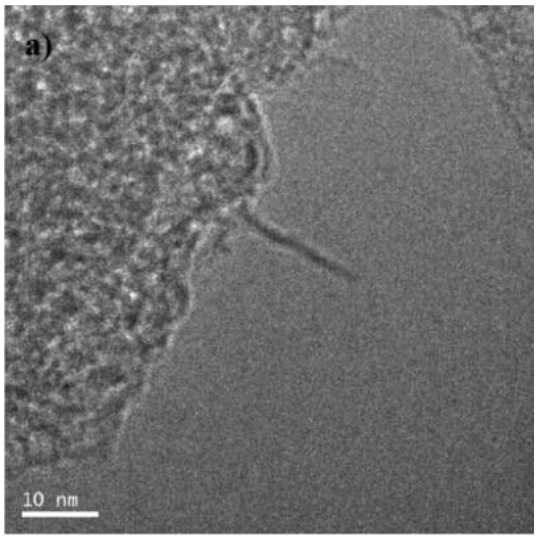

Figure 1.2 : Transmission electron microscopy (TEM) image of the first BNT synthesized in 2004 [15].

CNTs, which are successfully synthesized approximately one decade before graphene and regarded as a substantial driver for the scientific research on the nanomaterials, can be either metallic, semiconducting, or insulating depending on their radii and chiralities [18,19]. This generally suggests a weak control over the electronic properties of CNTs in specific applications [20]. Even though some reports claiming α-boron nanotubes (α-BNTs) with diameters less than 1.7 nm [21,22] or 2 nm [23] might show semiconducting behavior due to the band opening in Fermi level through curvature-induced out-of-plane buckling of certain atoms; subsequent calculations based on second-order Møller–Plesset perturbation theory [24] and dispersion-corrected density-functional calculations [25] and experimental studies [16] showed that the surface buckling might be an artifact of standard DFT. Thus, researchers concluded that, without surface buckling, all α-BNTs are indeed metallic [26]. In the same study, Bezugly et al. [27] conducted density functional studies on BNTs rolled from α-, 2-pmmn (buckled triangular) and distorted hexagonal sheet given in Figure 1.3, and reported that these BNTs are metallic, irrespective of their lattice types, radii and chiralities, and, highly conductive.

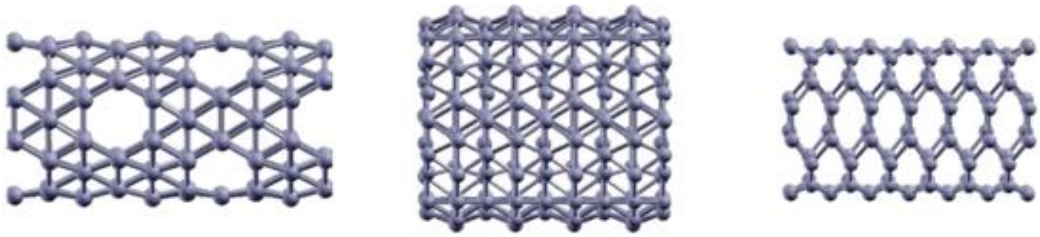

(a) (b) (c)

Figure 1.3 : BNTs which inspected by Bezugy et al. [27]. (a) α-BNT, (b) 2-pmmn BNT, and (c) distorted hexagonal BNT.

In a recent study, Wu et al. [28] have studied electron transport through BNTs rolled from β_{12}-borophene conducting DFT calculations and showed that the BNTs exhibit metallic behavior regardless of chirality and tube diameter, even though the atoms in the hexagonal centers are buckled. The fully metallic behavior of BNTs renders them appealing in the design of novel electronic nanodevices and hydrogen strorage [13]. In these applications, mechanical properties have a significant role since the mechanical strain is usually employed to modify the electronic properties of the BNTs [29]. Therefore, mechanical properties of the BNTs with different lattice structures such as tensile strength and elastic Young's modulus hold prominent importance.

1.2 Computational Methods

It is well known that in addition to their inherent uncertainties experimental methods are extremely complex and expensive to investigate the properties of nanostructured materials, which promotes numerical simulation techniques as promising alternatives [30]. In this regard, for the purpose of examining the mechanical, electrical, and chemical properties of BNTs there exist several numerical studies employing density functional theory (DFT) and molecular structural mechanics (MSM) techniques. For example, by performing DFT calculations, Tang and Ismail-Beigi [31] demonstrated that new boron sheets with mixed triangular and hexagonal lattices may exist. They also revealed that those boron sheets with non-zero hexagonal hole densities, i.e. η (ratio of the number of hexagon holes to the number of atoms in the original triangular sheet), are stable and can be the precursors of BNTs. Their predicted borophene models are given in Figure 1.4.

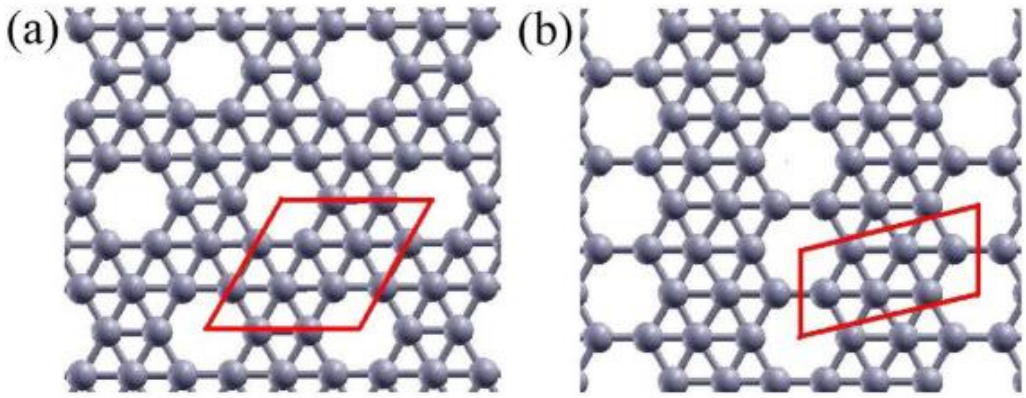

Figure 1.4 : Borophene sheets, predicted by Tang and Ismail-Beigi [31]. (a) α-borophene, (b) β-borophene. Unit cells of the are drawn with red.

Moreover, in a later work [23], they studied structural, energetic, and electronic properties of single- and double-layered boron sheets as well as single- and double-walled boron nanotubes by using the same method. Along the same line, Sebetci et al. [20] studied the structural, energetic, and electronic properties of the double-walled 2-pmmn BNTs ($\eta = 0$) by using DFT calculations and proved that the structures have metallic behavior. In a different study, Kunstmann and Quandt [32,33] explored the geometry, energetics, and basic chemical properties of 2-pmmn BNTs ($\eta = 0$) by conducting ab initio calculations and confirmed that zigzag BNTs with small diameters tend to have puckered surfaces. In another work, Kunstmann et al. [33] showed that the single-walled α-, 2-pmmn (buckled triangular) and distorted hexagonal BNTs were

thermally stable at synthesis temperature using DFT-based molecular dynamics. Regarding mechanical behavior, Evans et al. [34] studied mechanical properties of 2-pmmn BNTs using local density approximation (LDA) to density functional theory and calculated Young's moduli as 490 and 290 N/m in zigzag and armchair directions respectively. In a later work, Kochaev [35] investigated the elastic properties of BNTs with diameters between around 0.2 to 2 nm rolled from the 2-pmmn boron sheet ($\eta = 0$) by DFT calculations by presenting that Young's moduli of BNTs are around 1680 and 825 N/m for zigzag and armchair directions respectively. Researchers didn't comment on the difference of the values with the previous work. Besides that, not very long ago, Zhang and Zhou [36] studied the buckling characteristics of α-BNTs and χ-BNTs under axial compression using DFT-based MSM simulations and elastic continuum shell models. They noted that buckling mode transitions from shell buckling into column buckling can be observed with the increase in the aspect ratio. Recently, Aziz et al. [37] studied mechanical properties of 2-pmmn boron nanotubes using non-reactive molecular dynamics. They have used Stillinger-Weber (SW) potential field [38] to model the interactions between atoms, yet SW and some other potential fields are incapable of modeling BNTs for several reasons. The first one is that, even though it can successfully model the non-linear components, it is only applicable to the triangular phase of the borophene. Secondly, this three-body potential does not work for BNTs at room temperature, based on our preliminary simulations. Thus, they only simulated BNTs up to 100 K temperature.

1.3 Purpose of Thesis

Considering the studies in literature examining the physical behavior of BNTs, most of the theoretical studies regarding the boron nanotubes are based on the first-principles density functional theory (DFT) calculations. Although quantum mechanics-based DFT calculations provide fairly more accurate results compared to higher-level techniques such as classical molecular dynamics (MD), it is practically limited to the structures consisting of up to approximately 1000 atoms due to huge computational expense [38]. For this reason, classical MD simulations, which are widely utilized to explore the physical and chemical properties of nanostructured materials, can be used to investigate large systems with more than 1000 atoms as an alternative approach. In the present study, boron nanotubes are investigated using

reactive molecular dynamics simulations. Although reactive molecular dynamics has been extensively practiced for some borophene monolayers [30,39–43], to the best of our knowledge, it has not been used to simulate BNTs yet. In addition, we examined the mechanical properties of BNTs rolled from different borophene sheets (i.e. $\eta = 1/8\mathrm{b}, \eta = 4/27$) which remained almost unexplored. With this motivation, in this study, the mechanical properties of BNTs with different borophene allotropes are investigated by employing molecular dynamics simulations. Each BNT sample with different hexagonal hole densities are subjected to tensile loads at different strain rate levels. Mechanical characteristics including Young's modulus and ultimate strengths are evaluated and employed to make comparisons between different BNT types. In addition to the loading rates, the effects of temperature on the mechanical characteristics are also studied.

2. MOLECULAR DYNAMIC SIMULATIONS

In the present study, classical MD simulations are performed to investigate the mechanical properties of BNTs. Classical MD simulations are capable of modeling billions of atoms while quantum mechanics-based DFT simulations can only simulate models up to thousands of atoms.

The workflow of the molecular dynamics simulations is to calculate the trajectory of the particles. The particle positions should be given as input. The initial system is propagated by deterministic rules to generate a trajectory for each particle. Relevant information about the system can be taken for each timestep or also can be averaged over the entire trajectory. In molecular dynamic simulations, the equations of motion are integrated over time to generate the dynamical trajectory. Sub-atomic particles are not modeled in classical MD simulations. Thus, they have lower accuracy when compared with the quantum mechanics-based simulations. Some small systems might be suitable for quantum mechanics simulations, yet the vast majority of the molecular simulation studies require time and size scales that are not feasible with their high computational expense. [44]

Molecular simulation methods contain particles that have a mass and charge. The forces in the system are categorized as bonded interactions, which are calculated with the bond length, angle, and torsion, and non-bonded interactions such as electrostatic and van-der-Waals (vdW) forces. A potential energy function is assigned to each atom with many empirical parameters, usually derived from experiments or quantum mechanics simulations which are used to calculate the force of the bonded and non-bonded interactions. Potential energy functions are also called force fields in the context of molecular dynamics. The choice of the force field depends on the complexity of the simulated system. While two parameters might be enough for some systems, such as metal clusters, some might need complex fields to simulate even chemical reactions. However, complex force fields generally require high computational power. The accuracy of MD simulations is related to the precision of the force field [45].

2.1 Force Fields

There are multiple different force fields in molecular dynamics to model the interaction of the atoms. The most important terms of the total energy of an atomic system close to equilibrium can be given as follows [46]:

$$E_{sys} = E_{bond} + E_{angle} + E_{torsion} + E_{Vd\ Waals} + E_{Coulomb} \quad \textbf{(2.1)}$$

$$E_{bond} = k_b(r - r_0)^2 \quad \textbf{(2.2)}$$

$$E_{angle} = k_v(\varphi - \varphi_0)^2) \quad \textbf{(2.3)}$$

$$E_{\text{torsion}} = V_2(1 - \cos(2\omega)) + V_3(1 - \cos(3\omega)) \quad \textbf{(2.4)}$$

$$E_{\text{VdWaals}} = D_{ij}\left\{e^{\alpha_{ij}\left(1-\frac{r_{ij}}{r_{\text{VdW}}}\right)} - 2e^{\frac{1}{2}\alpha_{ij}\left(1-\frac{r_{ij}}{r_{\text{VdW}}}\right)}\right\} \quad \textbf{(2.5)}$$

$$E_{Coulomb} = C\frac{q_i q_j}{r_{ij}} \quad \textbf{(2.6)}$$

where E_{sys}, E_{bond}, E_{angle}, $E_{torsion}$, $E_{VdWaals}$ and $E_{Coulomb}$ are the energy of the system, bond, angle, torsion, and non-bonded van der Walls and Coulombic energies, respectively.

E_{bond}, E_{angle}, and $E_{torsion}$ terms in the total energy of the system are called bonded forces while $E_{VdWalls}$ and $E_{Coulomb}$ are called non-bonded forces. Hence, the total energy of the system can be simplified to

$$E_{sys} = E_{bonded} + E_{non\text{-}bonded} \quad \textbf{(2.7)}$$

One other such categorization can be defined by the number of atoms used in the force calculation, i.e. pairwise or many-body potentials.

This differentiation is one of the key separation points in which the physics of the system determines the important one. For example, a system composed of single atoms such as hydrogen or helium will not have any bonded interaction. Likewise, simulation of polymers, bonded atom chains will be heavily driven by bonded interactions.

2.1.1 Pairwise force fields

Pairwise force fields are the most basic approach for the modeling of atomistic systems. Lennard-Jones (LJ) force field, also called 6-12 Lennard-Jones potential, is a popular pairwise force field in which the force acting on an atom is calculated using:

$$E = 4\epsilon\left[\left(\frac{\sigma}{r}\right)^{12} - \left(\frac{\sigma}{r}\right)^{6}\right] \quad \textbf{(2.8)}$$

formula; where E is the energy, ϵ is the scaling factor for the bond energy, σ is the scaling factor for the distance and r is the distance between atoms.

Force fields can be used together in a system to represent different interactions. For instance, Coulombic forces can be added to the Lennard-Jones force field by calculating:

$$E_{Coulomb} = \frac{C q_i q_j}{\epsilon r} \quad \textbf{(2.9)}$$

where $E_{Coulomb}$ is the Coulombic energy, C is the constant for the energy conversion, q_i and q_j are the charges of atoms *i* and *j*, ϵ is the dielectric constant and r is the distance between atoms.

Another popular pairwise force field is the Buckingham force field in which the energy is calculated using

$$E_{Buckingham} = Ae^{-r/\rho} - \frac{C}{r^6} \quad \textbf{(2.10)}$$

where $E_{Buckingham}$ is the energy, A and C are constants related with the cutoff, r is the distance between atoms and ρ is the constant related with the ionic pair.

There are several other pairwise potentials such as Born-Mayer-Huggins potential.

2.1.2 Many-body potentials

Pairwise interactions are not able to model most of the systems in molecular dynamics. They are predominantly used in combination with the many-body potentials. Many-body potentials can calculate the energy with more than more atoms thus suitable for real systems. To give an example, embedded-atom method (EAM) potentials are popular for the modeling of metallic systems in which the energy is calculated using

[47]:

$$E_i = F_i\left(\sum_{j\neq i}\rho_\beta(r_{ij})\right) + \frac{1}{2}\sum_{j\neq i}\phi_{\alpha\beta}(r_{ij}) \qquad \textbf{(2.11)}$$

where the energy of the atom i is the E_i, F_i is the embedding energy, first summation terms represent the electron density of the environment, and the second energy term represents pairwise interactions.

There are several other force fields specific to the nature of the system. For example, a very popular version of the EAM potential is called the modified embedded atom method (MEAM) [48] which also includes the angular forces.

Another popular non-linear many-body potential is the Stillinger-Weber (SW) [49] potential in which the energy of the system of atoms calculated as

$$E = \sum_i \sum_{j>i} \phi_2(r_{ij}) + \sum_i \sum_{j\neq i} \sum_{k>j} \phi_3(r_{ij}, r_{ik}, \theta_{ijk}) \qquad \textbf{(2.12)}$$

where E is the energy of the system and the functionals ϕ_2 and ϕ_3 are used to calculate the two-body and three-body forces.

While force fields such as MEAM and SW might not capable of modeling complex systems such as organic or biomolecules, there are several universal force fields, meaning that they can represent the molecules as a group or such systems that have numerous elements in their structures such as proteins or nucleic acids. Force fields for biological systems worth mentioning are CHARMM [50], AMBER [51], UFF [52], and DREIDING [53]. These force fields generally use the equations given in equations 2.1 to 2.7.

Force fields mentioned to this point are not capable of chemical reactivity or different bond states in a system. Fortunately, there are two exceptionally successful force fields for the simulation of systems containing different bond orders of the same atom called Adaptive Intermolecular Reactive Empirical Bond Order (AIREBO) Potential [54] and ReaxFF. These force fields take into account the breaking and the formation of the bonds. The bond order (BO) concept in these force fields allow the local chemical environment to be considered in their formulation which in turn lets the simulation of

different hybridizations such as sp, sp^2, and sp^3.

AIREBO potential is based on Reactive Empirical Bond Order (REBO) [55] potential calculates the energy of the systems as

$$E = \frac{1}{2}\sum_{i}\sum_{j\neq i}\left[E_{ij}^{\mathrm{REBO}} + E_{ij}^{\mathrm{LJ}} + \sum_{k\neq i,j}\sum_{l\neq i,j,k} E_{kijl}^{\mathrm{TORSION}}\right] \quad \textbf{(2.13)}$$

where the second and third terms correspond to the Lennard-Jones and torsional terms while the first term is called chemical binding energy and is calculated as

$$E_{ij}^{\mathrm{REBO}} = V_{ij}^{\mathrm{R}}(r_{ij}) + b_{ij}V_{ij}^{\mathrm{A}}(r_{ij}) \quad \textbf{(2.14)}$$

where the functionals V^R and V^A are used to calculate the repulsive and attractive forces by valance electrons, respectively. b_{ij} corresponds to the empirical bond order function.

The main drawback of the AIREBO force field is the capability of modeling different elements. This force field can only model the carbon and hydrogen atoms. Even further, the ReaxFF force field can be beneficial for the modeling of the systems since it can utilize long-range exponentially decaying bond order per bond distance without cutoff. In AIREBO, the distance for covalent bonds is limited to 2 Å [56].

2.1.3 ReaxFF

ReaxFF is a reactive bond order potential allowing different hybridizations and chemical reactivity. In ReaxFF, the overall energy is calculated as [57]

$$\begin{aligned} E_{\mathrm{system}} = {} & E_{\mathrm{bond}} + E_{angle} + E_{\mathrm{tors}} + E_{\mathrm{vdWaals}} + E_{\mathrm{Coulomb}} + E_{C2} + E_{\mathrm{over}} \\ & + E_{\mathrm{pen}} + E_{\mathrm{coa}} + E_{\mathrm{triple}} + E_{\mathrm{under}} + E_{\mathrm{val}} + E_{\mathrm{conj}} + E_{H-\mathrm{bond}} + E_{lp} \end{aligned} \quad \textbf{(2.15)}$$

where E_{bond}, E_{angle}, $E_{torsion}$, $E_{vdWalls}$, and $E_{Coulomb}$ energies are calculated using bond orders unlike given in Equations 2.2 to 2.6, while E_{C2} is the correction term to capture the stability of C=C, E_{over} and E_{under} are the over-coordination and under-coordination terms to impose an energy penalty for incorrect bond orders, E_{pen} is the penalty energy to correct the stability of systems in which with two double bonds in a valency angle, E_{coa} is the angle conjugation term to stabilize NO_2 group, E_{triple} is the triple bond stabilization energy, E_{val} is the valance angle energy, E_{conj} is the four body conjugation

energy, $E_{H\text{-}bond}$ is the hydrogen bond energy, and E_{lp} is the lone pair energy. Some of these terms can be neglected based on the dynamics of the system.

The interactions between the boron atoms are modeled using a reactive force field known as ReaxFF permitting continuous bond formation/breaking and developed by Adri van Duin et al. [58]. $ReaxFF_{CBN}$ parametrization has been developed by Pai et al. [59] for the simulation of liquid carbon-boron-nitrogen materials which provides remarkably accurate results with respect to the first principles predictions available in the literature [30,41]. In literature, some other potentials are used to examine boron-based nanostructures. For instance, Zhou et al. has developed a non-reactive force field (Stillinger-Weber potential) [38] which is only capable of representing force field in 2-pmmn ($\eta = 0$) quasi-planar structure. In this regard, there are no force fields to represent all of the allotropes of borophene sheets other than ReaxFF within the knowledge of the authors.

2.2 Statistical Ensembles

Macroscopic thermodynamic properties like temperature, pressure, density or heat capacity, and microscopic properties such as specific free energy differences in molecules should be estimated in molecular dynamic simulations. Connections of macroscopic properties and atomic properties such as velocity can be made through statistical thermodynamics. Several thermodynamics ensembles can be utilized to control the system in molecular dynamics. The main function of an ensemble is to keep the system in the desired state point such as in a targeted temperature and pressure in a varying volume. The key point is maintaining desired properties while also keeping the system in a non-biased state to the initial conditions.

Ensembles are generally named after their control parameters. Commonly used ensembles in molecular dynamics are Canonical (NVT, constants: number of particles, volume, and temperature), Grand Canonical (μVT, constants: chemical potential, volume, and temperature), Micro Canonical (NVE, constants: number of particles, volume, and energy) and isothermal-isobaric (NPT, constants: number of particles, volume, and pressure).

There are several mathematical formulations to maintain the targeted temperature or pressure called thermostats or barostats, respectively. Thermostats and barostats can

be categorized in several ways. For example, depending on the use of random numbers in the guidance of the dynamics, they can be categorized as deterministic or stochastic. As another example, they can be coupled to the entire system or to a small subset, which determines if they are global or local. They might also be categorized by their formulation. For instance, the integrator update positions and momenta of the particles, and the thermostat rescales the velocities to maintain the temperature. On the other hand, some thermostats or barostats act as a temperature or pressure bath outside the system by adding additional degrees of freedom to the equations of motion.

Gaussian, simple velocity scaling, Berendsen, Bussi-Donadio-Parinello, Andersen, Langevin, and Nosé-Hoover thermostats and simple volume rescaling, Berendsen, Andersen, Parinello-Rahman, Martyna-Tuckerman-Tobias-Klein barostats are some of the most popular formulations. Refer to Braun et al. [45] for further reading.

2.3 Time Integration

Molecular dynamics simulations employ classical mechanics as explained before. There are several mathematical formulations in classical mechanics such as Newtonian, Hamiltonian, and Lagrangian. The choice of the formulation depends on the application yet they are physically equivalent. However, many methods use the Hamiltonian formulation.

The basic concept of the MD method is to generate successive, deterministic configurations of an isolated system. Newton's equation of motion describes the evolution of the system as follows:

$$\frac{d\mathbf{p}_i}{dt} = -\frac{\partial U(\mathbf{r}^N)}{\partial \mathbf{r}_i} \text{ for all } i \tag{2.16}$$

or alternatively:

$$\frac{d\mathbf{p}^N}{dt} = -\nabla U(\mathbf{r}^N) \tag{2.17}$$

where p is the momentum and r is the coordinates of atoms, and U is the potential energy where a set of 3N second-order, nonlinear, coupled partial differential equations is described.

The trajectory and Equation 2.17 are solved in a discrete-time approximation with steps in time. The forces on each atom and the configuration at the next time step are calculated for each timestep. With this approach, the atomic positions of the system are acquired at specific time intervals, such as $r^N(0)$, $r^N(\delta t)$, $r^N(2\delta t)$ …, where δt is the time step. Equations of motion become accurate with the decreasing time step for computational expense and shorter simulation time.

Time stepping of the continuous position function $r^N(t)$ can be calculated using the Taylor expansion for an increment in time δt from the current time t of the position vector r which gives

$$\begin{aligned} r(t+\delta t) &= r(t) + \frac{dr(t)}{dt}\delta t + \frac{d^2r(t)}{dt^2}\frac{\delta t^2}{2} + \frac{d^3r(t)}{dt^3}\frac{\delta t^3}{6} + \vartheta(\delta t^4) \\ &= r(t) + v(t)\delta t + \frac{f(t)}{m}\frac{\delta t^2}{2} + \frac{d^3r(t)}{dt^3}\frac{\delta t^3}{6} + \vartheta(\delta t^4) \end{aligned} \quad \textbf{(2.18)}$$

and similarly for the step backward,

$$r(t-\delta t) = r(t) - v(t)\delta t + \frac{f(t)}{m}\frac{\delta t^2}{2} - \frac{d^3r(t)}{dt^3}\frac{\delta t^3}{6} + \vartheta(\delta t^4) \quad \textbf{(2.19)}$$

An equation that predicts the atomic position at the next step can be obtained by adding Equations 2.18 and 2.19 and moving the $r^N(t-\delta t)$ to the right-hand side,

$$r(t+\delta t) = 2r(t) - r(t-\delta t) + \frac{f(t)}{m}\delta t^2 + \vartheta(\delta t^4) \quad \textbf{(2.20)}$$

Equation 2.20 is called the Verlet algorithm. An alternative is called velocity Verlet algorithm and formulated with two equations as follows

$$\begin{aligned} r(t+\delta t) &= r(t) + v(t)\delta t + \frac{f(t)}{2m}\delta t^2 \\ v(t+\delta t) &= v(t) + \frac{f(t+\delta t) + f(t)}{2m}\delta t \end{aligned} \quad \textbf{(2.21)}$$

This algorithm only requires one set of positions and velocities at each time step. With this advantage, it is one of the most popular time integrators in molecular dynamic simulations.

3. METHODOLOGY

3.1 Atomistic Modelling

In this study, some computer codes are developed to generate the initial configuration of the borophene structures and then to transform them into BNTs. A sample code for BNT generation is provided in Appendix A1. Borophene analogs of the BNTs are categorized after their direction of rolling. As illustrated in Figure 3.1, if the sheet rolled around perpendicular to the zigzag path, the tube takes the name zigzag, similarly, armchair for the perpendicular to the armchair path.

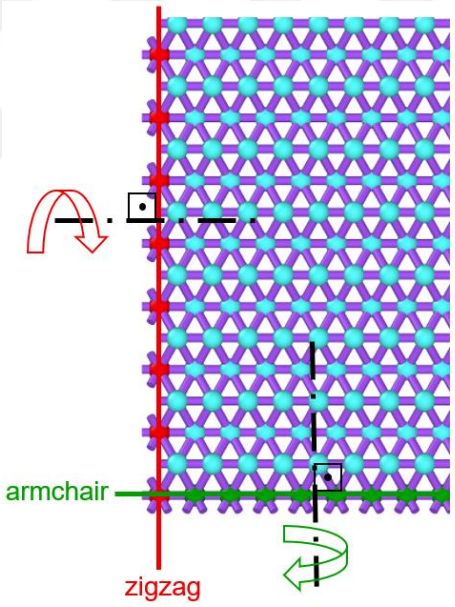

Figure 3.1 : Chiral names of nanotubes by direction of rolling.

We investigated 10 different boron nanotube configurations in this study. 2-pmmn is the only quasi-planar structure and it is illustrated in Figure 3.2 with its top and side views. The other structures are planar and given in Figures 3.3 (β group, (a) $\beta_{12,}$ (b) $\beta_{13,}$ (c) β_4 and (d) β_5), 3.4 ((a) χ_3, (b) α and (c) δ_3) and 3.5 ((a) $\eta_{1/8b}$ and (b) $\eta_{4/27}$)

Lattice parameters are taken as 1.614, 2.866, and 0.911 Å in *a*, *b*, and *h* directions for quasi-planar structures [60] and 2.926 and 5.608 Å for planar structures [61], respectively.

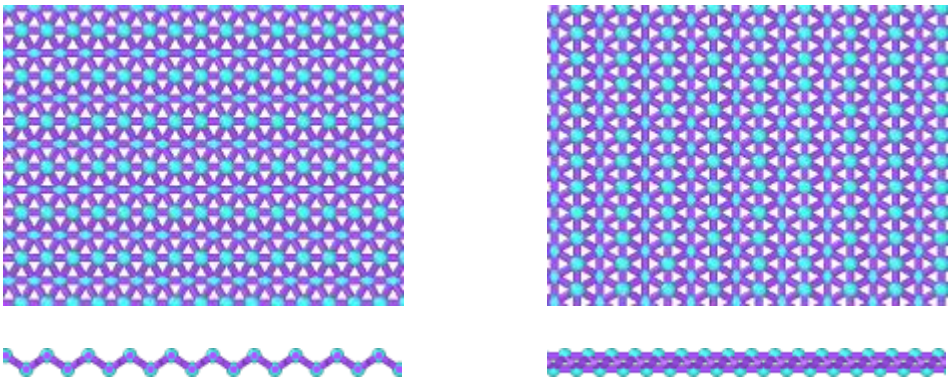

(a) (b)

Figure 3.2 :2-pmmn quasi-planar borophene structure. (a) zigzag direction and (b) armchair direction horizontally.

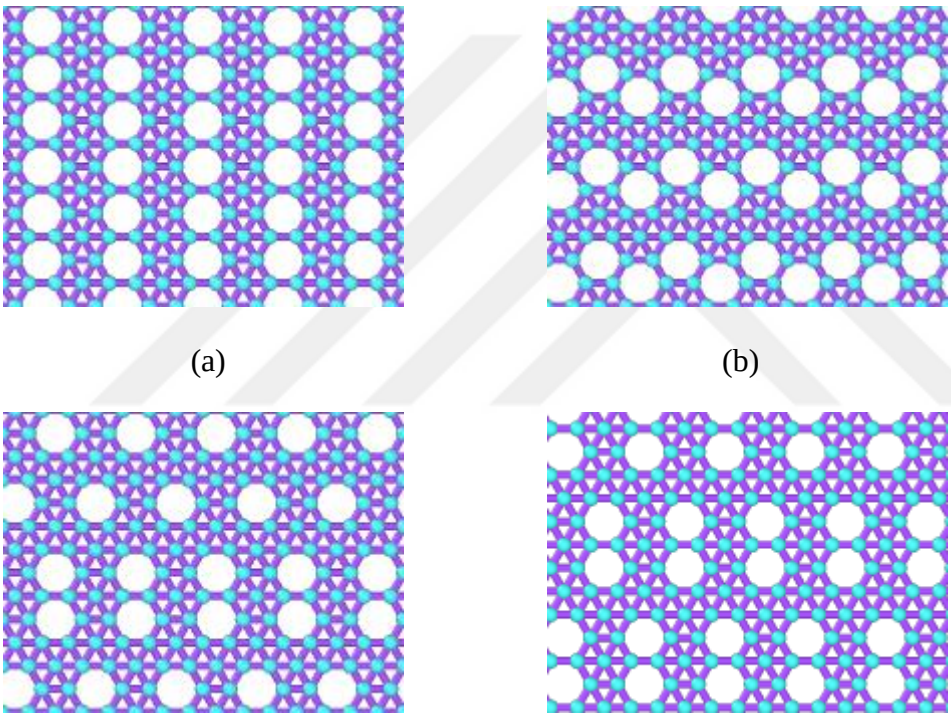

(a) (b)

(c) (d)

Figure 3.3 : Structures in β group. (a) $\beta_{12,}$ (b) $\beta_{13,}$ (c) β_4 and (d) β_5.

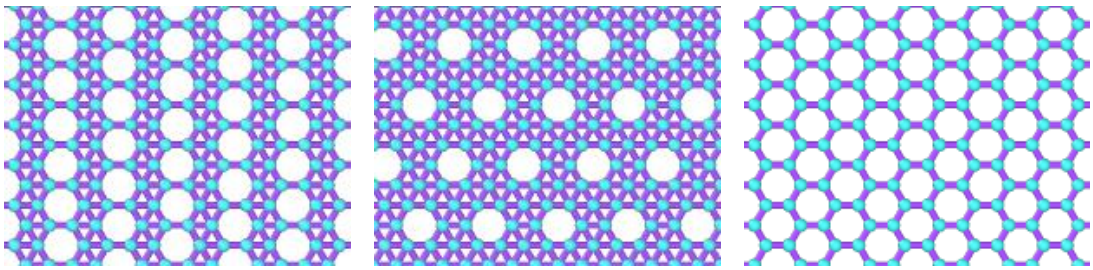

(a) (b) (c)

Figure 3.4 : Other planar borophene structures. (a) χ_3, (b) α and (c) δ_3

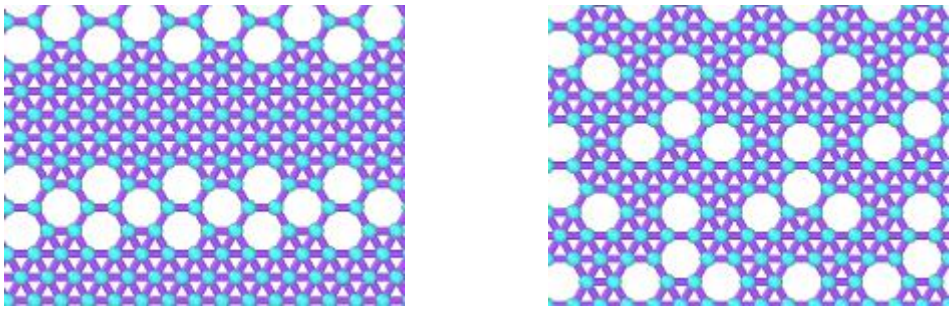

(a) (b)

Figure 3.5 :(a) $\eta_{1/8b}$ and (b) $\eta_{4/27}$ borophenes.

Generated nanotubes are illustrated in Figure 3.6. The diameters and lengths of the structures are given in Table 3.1.

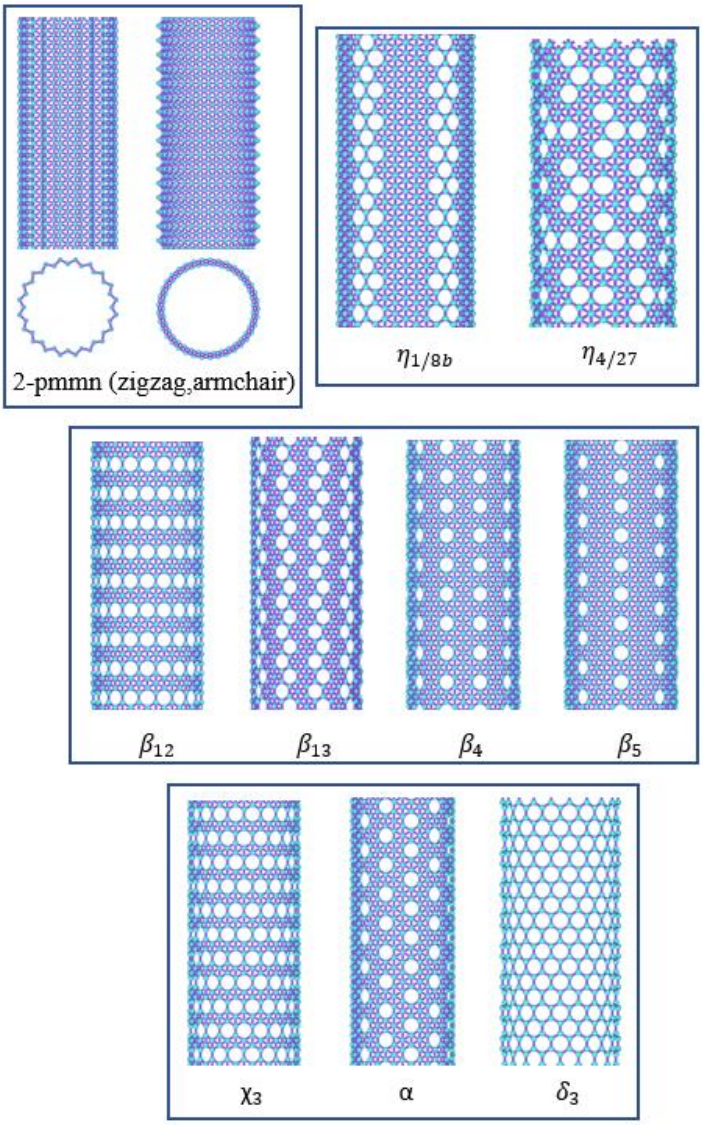

Figure 3.6 :BNTs that were studied in this work. Planar structures are in zigzag direction.

Table 3.1 : Diameters and lengths of structures.

Structure		Diameter	Length	Aspect ratio
2-pmmn	Zigzag	1.85	5.73	6.21
	Armchair	1.99	5.59	5.62
$\boldsymbol{\beta_{12}}$	Zigzag	1.86	5.41	5.80
	Armchair	1.77	5.71	6.43
$\boldsymbol{\beta_{13}}$	Zigzag	1.86	5.49	5.89
	Armchair	1.77	5.71	6.43
$\boldsymbol{\beta_{4}}$	Zigzag	1.86	5.49	5.89
	Armchair	1.77	5.71	6.43
$\boldsymbol{\beta_{5}}$	Zigzag	1.86	5.49	5.89
	Armchair	1.77	5.71	6.43
χ_{3}	Zigzag	1.86	5.74	6.17
	Armchair	1.88	5.71	6.06
α	Zigzag	1.68	5.49	6.55
	Armchair	1.77	5.12	5.77
$\boldsymbol{\delta_{3}}$	Zigzag	1.86	4.90	5.26
	Armchair	1.61	5.71	7.07
$\boldsymbol{\eta_{1/8b}}$	Zigzag	1.86	5.49	5.89
	Armchair	1.77	5.71	6.43
$\boldsymbol{\eta_{4/27}}$	Zigzag	1.68	4.48	5.34
	Armchair	1.45	5.12	7.05

3.2 Overview of LAMMPS

Large-Scale Atomic/Molecular Massively Parallel Simulator (LAMMPS) is an open-source code developed by Sandia National Laboratories [62]. This code is specifically designed for multi-core computer architectures. It can use several parallelism options such as Message Passing Interface (MPI), shared memory parallelism (OpenMP multi-threading), vectorization, Compute Unified Device Architecture (CUDA), and many other performance packages.

LAMMPS is capable of modeling atomic, polyatomic, polymeric, biological, metallic, solid-state, coarse-grained, granular and many other systems with utilizing a wide variety of force fields such as ReaxFF for reactive molecular dynamics, CHARMM for proteins and nucleic acids, EAM for solid-state metallic materials, AIREBO for carbon allotropes, LJ for vdW interactions, in general.

The general working principles of LAMMPS follow the MD principles explained in Section 2. Specifically, this program utilizes neighbor lists, lists that contain relevant atoms for force calculations, and spatial decomposition for parallelism.

We utilized several versions of LAMMPS with numerous numbers of compilers to benchmark our problem in our workstation and two different clusters, UHeM and TRUBA. Generally, we worked on Intel processors using Sandy Bridge, Broadwell, and Skylake architectures.

We used ReaxFF and ReaxC-OMP packages, implemented by Aktulga et al.[63,64]. Our benchmark results indicate that the choice of the compiler has up to around 20% performance effect on calculation speed. The choice of parallel computing method should be benchmarked for every specific problem, version of the program, and processor architecture. The speed might increase many times in some situations with the suitable method. For our case, we get the best performance using hybrid (MPI and OpenMP) in Sandy Bridge for most of our workflows. However, for newer generation architectures with the latest version of LAMMPS compiled using Intel's Low-Level Virtual Machine (LLVM) compiler (icx), the distributed memory approach (MPI) yielded around 50% better performance for the main workflow of our simulations, when compared with the hybrid method. Our observations indicate that, with a specific configuration, performance might increase in the thermalization part, while it can decrease in the mechanical tension/compression section of the simulation or vice versa.

Therefore, every part of the problem should be treated separately while seeking the best performance. Benchmarking should be conducted for every different problem and for every configuration of LAMMPS to achieve the fastest computing speed.

A sample input script used in this work can be found in Appendix A2.

3.3 Energy Minimization

In molecular dynamics, the energy of the system should be at the local minimum to avoid unwanted artifacts. The forces might increase to unreasonable levels with slight changes in the position of atoms which might result in large displacements. While there are some non-derivative minimization methods such as Simplex and sequential univariate, the most popular energy minimization methods are derivative methods.

Typical energy minimization methods are the steepest descent, line search, arbitrary step, and conjugate-gradient (CG) for the first order, and the Newton-Raphson, Quasi-Newton methods for the second order.

We used the Polak-Ribiere version CG method [65] in which the force gradient is combined with previous information to find the direction of the conjugate [66].

3.4 Thermalization and Mechanical Strain

MD simulations are conducted LAMMPS [62], with velocity Verlet time-integration algorithm. The periodic boundary condition is applied in the longitudinal direction for the avoidance of the boundary effects. For boron nanotubes, 50 A˚ vacua are defined for the lateral (i.e. radial) directions. The specimens are relaxed to zero stress state with NPT ensemble using the Nose´-Hoover barostat and thermostat method for 1 ps. Uniaxial tension and compression tests are carried out by applying constant engineering strain rates of $1\ x\ 10^{9}, 1\ x\ 10^{10}, 1\ x\ 10^{11}$ (1/s) so that the loading rate is calculated using the engineering strain rate and the simulation box size. The size of the simulation box along the direction perpendicular to the loading (i.e. longitudinal) direction is controlled with the assumption of NPT ensemble to achieve zero stress condition along the edge lateral to the loading direction to guarantee uniaxial stress conditions.

Macroscopic stress tensor is estimated by using the virial stress theorem as given in

Eqn. 3.1 [30]

$$\sigma = \frac{1}{V}\sum_{i \in V}\left[-m^{(i)}v^{(i)} \otimes v^{(i)} + \frac{1}{2}\sum_{i \neq j} r^{(ij)} \otimes f^{(ij)}\right] \quad \textbf{(3.1)}$$

where $m^{(i)}, v^{(i)}\, r^{(i)}, r^{(ij)}, f^{(ij)}$ and V are the mass and velocity vector of the atom, the position of the atom *i*, the distance vector between the atoms i and *j*, the interatomic force applied on atom a by atom b, and the volume of the structure, respectively. The thickness of the boron films is reported as 2.9[8], 3[67], 4.2 [68], and 5[69] Å in recent experimental studies. Due to this ambiguity, we submit Young's modulus and stress values in the form of $E \cdot t$ and $\sigma \cdot t$, respectively, where t is the thickness.

The engineering strain is calculated as:

$$\varepsilon^{t} = \frac{L_x^t - L_x^0}{L_x^0} \quad \textbf{(3.2)}$$

where ε^t and l_x^t is the engineering strain and length along longitudinal (i.e. *x*) direction at the instant respectively and L_x^0 is the initial length along the *x*-direction.

4. RESULTS AND DISCUSSION

4.1 Energy Minimization and Thermalization Characteristics of BNTs

Based on the results, we report that the ReaxFF potential field can successfully minimize the structures. These structures are also can stay thermally stable under an isothermal-isobaric ensemble when modeled with the ReaxFF force field. Our results indicate that the lattice parameters change similar to the borophene, as shown by Mortazavi et al. [40]. Even though, they reported that simulation results were not affected by this inaccuracy of the potential field. We observed a similar situation regarding BNTs. The simulation box increases in size by 10% and 20% in axial and radial directions respectively. The elliptic cross-section is a structural property of BNTs due to the bands in the Fermi level. The details of this property are explained by Kunstmann et al. [26]. In their article, using DFT simulations, they observed that energy minimized BNTs take an elliptic shape. Our results are confirmed with DFT simulations, which is an indicator of the capability of ReaxFF for the simulation of BNTs. The change of the shape is given in Figure 4.1. Another common structural property of BNTs is the surface buckling of atoms in the hexagonal center. Surface buckling is reported by Tang and Ismail-Beigi [23] in their first-principles study. ReaxFF force field can also represent the surface buckling property of BNTs. The change of radius by atoms is given in Figure 4.2. These structural similarities imply that the ReaxFF force field is capable of representing key structural features of BNTs.

Figure 4.1 : Initial (gray) and final (red) structures of BNTs during energy minimization. α-BNT is given as an example.

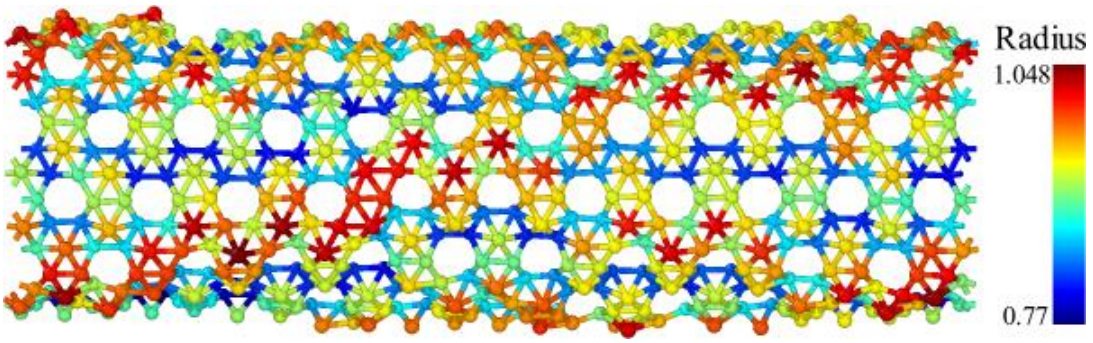

Figure 4.2 : Change of radius by atom in BNT after thermalization for 1 ps at 1 K. α-BNT zigzag is given as an example.

After thermalization, there are several different types of cross-section for the BNTs, depending on the configuration, given in Figure 4.3. The shape of the cross-section is an important indicator of mechanical behavior.

The potential energy distribution is the main driving force for these differences. If the potential energy is evenly distributed, the structure can preserve the homogeneous shape, which results in more brittle behavior during the tensile.

For example, the 2-pmmn zigzag cross-section, given in Figure 4.3a, is the most homogeneous in terms of potential energy. This structure is highly brittle and has the highest Young's moduli, thus the stiffest structure. Another example is the β_{12} zigzag structure, given in Figure 4.3b. In this one, the potential energy is not homogeneous as the 2-pmmn yet the distribution is small enough that it can form a semi-circular shape. However, some structures, such as β_{13}, given in Figure 4.3c, have a high potential energy gradient, thus the cross-section has a ring shape. This type of cross-section results in a more ductile tensile behavior. Finally, the last type is the rectangle-like cross-section like β_5, given in Figure 4.3d. These structures tend to behave in between brittle and ductile fractures. They can still carry some load after ultimate tensile stress, but not as much as the ductile behaving structures like β_{13}.

The cross-section evolves to different kinds of shapes due to the Poisson effect which is later explored in detail in the following sections. The main impact of this effect is the bond formation due to contraction. The direction and the stability and/or instability of these forming/deforming bonds determine the mechanical response of the material.

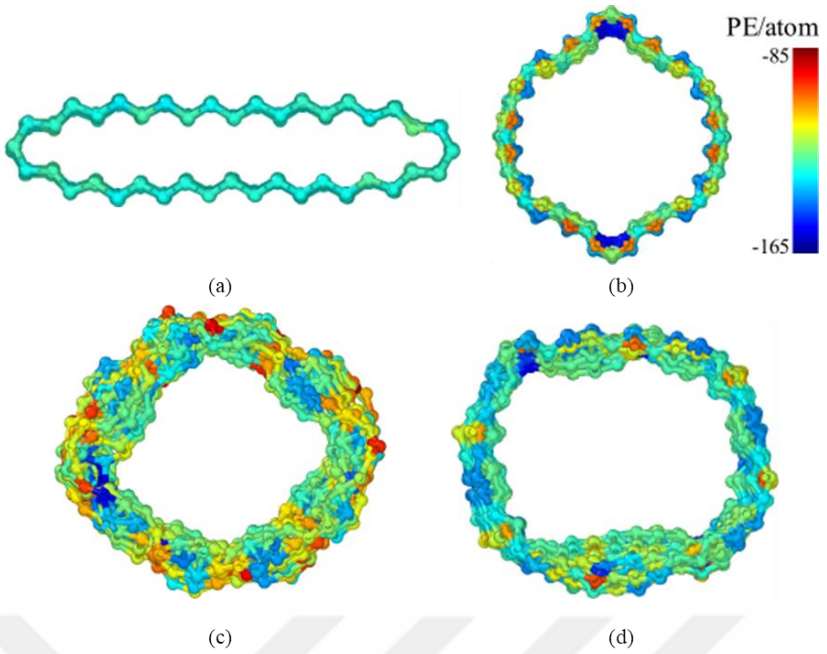

Figure 4.3 : Cross-section of the structures after thermalisation at 300 K. (a) 2-pmmn, (b) β_{12}, (c) β_{13}, (d) β_5 zigzag configurations.

4.2 Mechanical Characterization of Boron Nanotubes

Stress-strain curves of twenty different BNT configurations at 1K and the room temperature are given in Figure 4.4. To provide a quantitative examination, numerical values for several mechanical characteristics of all configurations including ultimate tensile stress, strain, and Young's moduli calculated at three different temperatures (i.e. 1 K, 300 K, and 600 K) are also given in Table 4.1. Amongst all BNT structures, it is seen that the zigzag configuration of the 2-pmmn structure has much higher stiffness and ultimate tensile strength compared to the other BNTs, while its ultimate strain is much less than most of the other structures due to high brittleness. Furthermore, it can be also noted that depending on the configuration, significant distinctions between the armchair and zigzag directions are observed for some BNTs including 2-pmmn, δ_3, and χ_3. The main reason for this distinction is the configurational dissimilarities of bond and/or hole arrangements along with different directions. Considering the stress-strain curves of zigzag and armchair directions for each BNT type, $\eta_{4/27}$ structure has the highest isotropy for the armchair and zigzag directions.

The numerical values for the ultimate tensile stress, strain, and Young's moduli are given in Table 4.1.

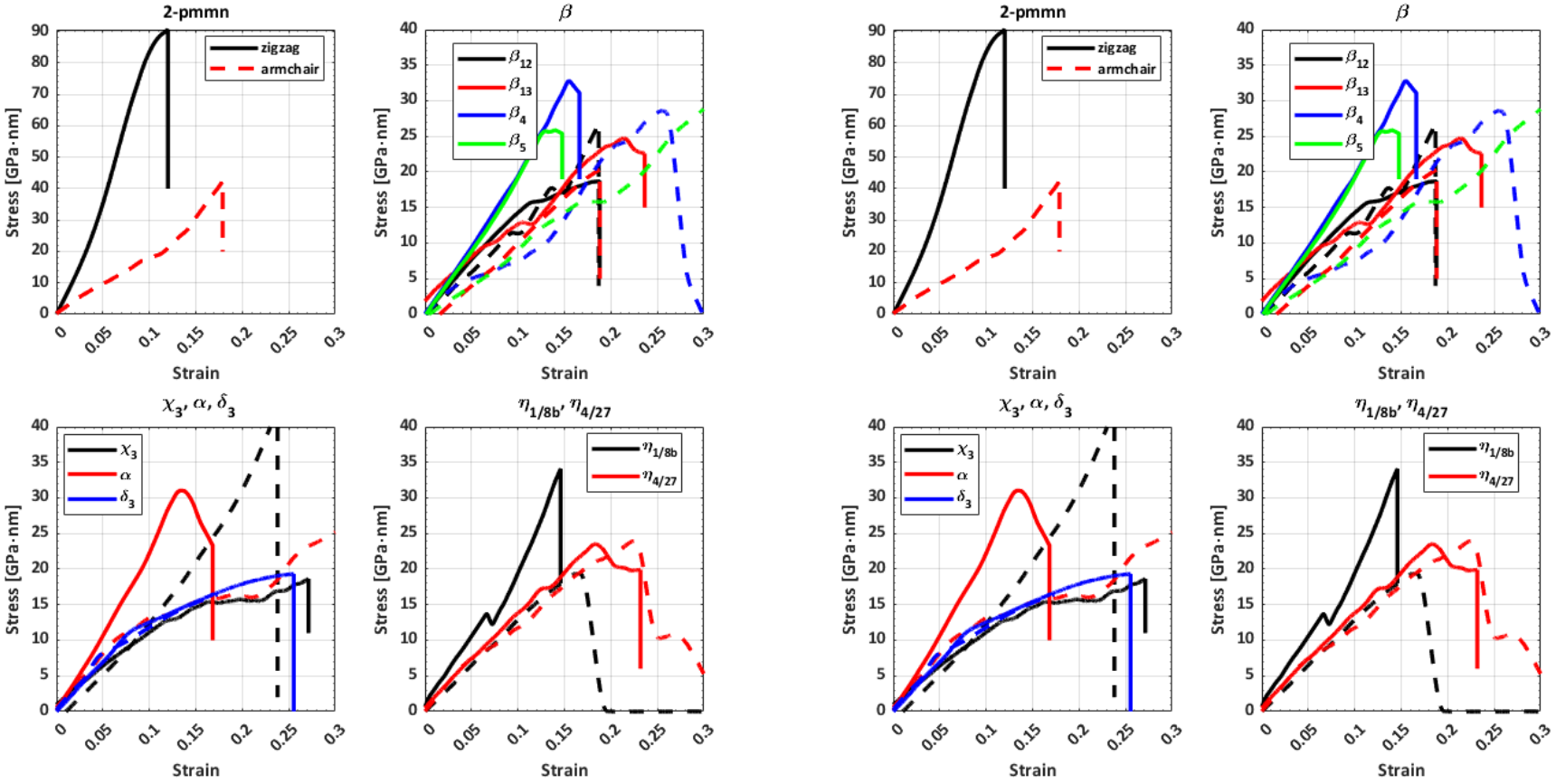

Figure 4.4 : Stress-strain comparison for BNTs at (a) 1 K and (b) 300 K, straight lines are zigzag, and dashed lines are armchair configurations.

Table 4.1 : Ultimate tensile stress, strain, and Young's moduli for structures.

Structure	Chirality	Temperature [K]	Ultimate Tensile Stress [GPa·nm]	Ultimate Tensile Strain	Young's Modulus [GPa·nm]
2-pmmn	Zigzag	1	90.66	0.1201	723
		300	76.11	0.0925	708.2
		600	61.32	0.0776	706.2
	Armchair	1	42.44	0.179	194.6
		300	33.87	0.1686	218.7
		600	21.73	0.1512	194.7
$\boldsymbol{\beta_{12}}$	Zigzag	1	18.7	0.1881	152.8
		300	21.83	0.2189	93.16
		600	15.57	0.2039	73.56
	Armchair	1	26.71	0.187	119.4
		300	22.2	0.1637	131.5
		600	16.59	0.1535	135.1
$\boldsymbol{\beta_{13}}$	Zigzag	1	24.74	0.2146	147.7
		300	16.08	0.2433	139.8
		600	13.28	0.1858	140.1
	Armchair	1	20.36	0.1882	77.7
		300	15.65	0.1635	114.1
		600	12.97	0.2049	93.68
$\boldsymbol{\beta_4}$	Zigzag	1	32.76	0.155	189.2
		300	25.02	0.1445	176
		600	20.38	0.1306	177.9
	Armchair	1	28.59	0.2554	99
		300	24.9	0.2515	86.64
		600	16.39	0.2452	104
$\boldsymbol{\beta_5}$	Zigzag	1	25.85	0.1402	177.6
		300	19.31	0.13	158.4
		600	16.67	0.1155	153.6
	Armchair	1	28.83	0.3001	78.68
		300	19.75	0.1869	120.7
		600	17.95	0.1539	111.5
$\boldsymbol{\chi_3}$	Zigzag	1	18.66	0.2715	128.1
		300	15.08	0.2266	108.4
		600	11.9	0.2738	104.2
	Armchair	1	42.51	0.2382	101.3
		300	26.92	0.1834	177.2
		600	16.44	0.1844	153.2
$\boldsymbol{\alpha}$	Zigzag	1	31.03	0.1347	213.9
		300	25.56	0.1316	174.4
		600	20.59	0.1245	154.6
	Armchair	1	25.24	0.3001	162.8
		300	21.1	0.2542	105.8
		600	17.72	0.2161	106.5

Table 4.1 (continued): Ultimate tensile stress, strain, and Young's moduli for structures.

Structure	Chirality	Temperature [K]	Ultimate Tensile Stress [GPa]	Ultimate Tensile Strain	Young's Modulus [GPa]
δ_3	Zigzag	1	19.32	0.2556	140.4
		300	18.27	0.2306	124.9
		600	17.07	0.2214	103.5
	Armchair	1	16.46	0.1731	153
		300	11.02	0.0862	188.2
		600	12.19	0.1133	169.5
$\eta_{1/8b}$	Zigzag	1	34.1	0.1461	212.6
		300	22.57	0.1453	174.9
		600	20.46	0.1619	142
	Armchair	1	19.39	0.165	129.4
		300	13.92	0.1296	115.4
		600	15.67	0.1452	137.4
$\eta_{4/27}$	Zigzag	1	23.53	0.1835	148.5
		300	18.59	0.1905	105
		600	15.53	0.1864	91.12
	Armchair	1	23.94	0.225	144.4
		300	18.47	0.2159	90.47
		600	14.38	0.1721	99.42

From Figure 4.4 and Table 4.1, it can be observed that the 2-pmmn zigzag configuration has the highest fracture stress and Young's modulus among BNTs. If the thickness of the BNT is taken as 2.9 Å [40], the ultimate tensile stress and Young's modulus take the values of around 262 GPa and 2442 GPa respectively which are almost equal to the 2.5 times of those seen in CNTs [70]. Furthermore, all BNT structures have tensile stress values comparable to various configurations of CNTs, even though having vacancy defects in the configuration. Besides, some configurations are more ductile than most of the CNTs.

In Figure 4.5, the ultimate tensile stress of the structures is plotted against their vacancy ratio. Some structures, such as β_4 and $\eta_{1/8b}$ have the same vacancy ratio but different mechanical stress values. This difference is increasing with the increase in the vacancy ratio. Thus, it can be concluded that the mechanical properties become more dependent on the atomistic configuration as the vacancy ratio increases.

For different strain rates, Young's moduli of the structures don't change yet the ultimate tensile stress slightly increases. We continued with 10^9 1/s strain rate for the rest of the results. Comparisons of the stress-strain curves are given in Appendix A3.

The size of the nanotubes also has almost no effect on the stress-strain plots. Several

examples with lengths of 6, 10, and 15 nm, and diameters around 2 and 5 nm are given in Appendix A3.

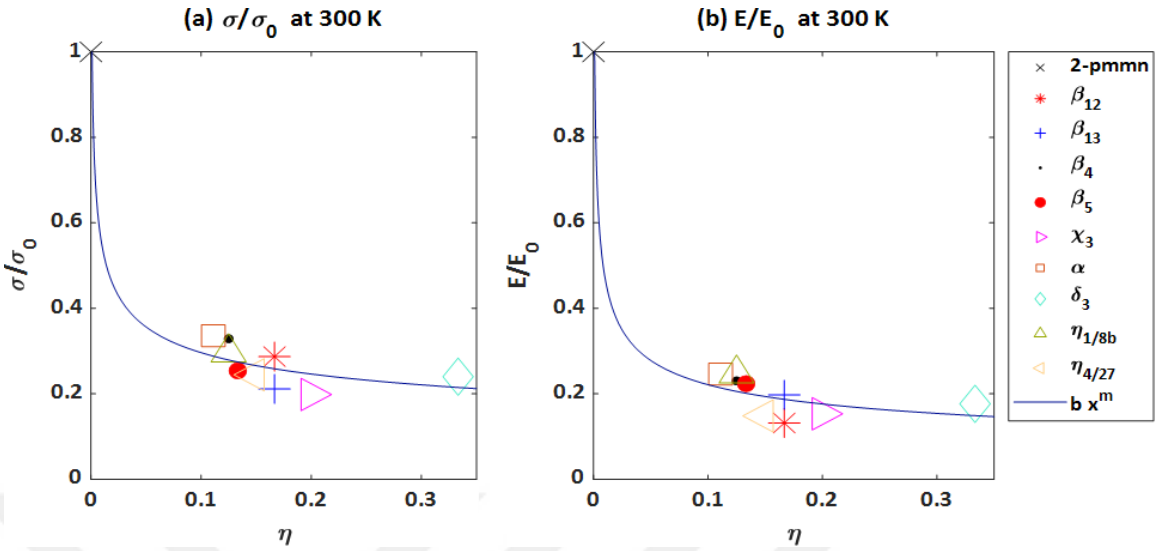

Figure 4.5 : (a) Change of ultimate tensile stress and (b) change of Young's moduli of structures with respect to the vacancy ratio, η.

Excluding the out-of-plane structure (i.e. 2-pmmn), all the other planar BNT structures can be considered as nanoporous structures due to having a non-zero vacancy ratio. It is very well known that the effective mechanical properties of the cellular bulk solids highly depend on the relative density which is defined as the ratio of the densities of the cellular solid and bulk solid. Considering the analogy between the relative density and the vacancy ratio, it can be noted that Young's moduli and the ultimate tensile strength of porous BNT structures tend to decrease with increasing vacancy ratio (see Figure 4.5 :). Moreover, it is also noticed that vacancy ratio is not the only parameter affecting the mechanical behavior of BNTs. For instance, although the BNTs β_4 and $\eta_{1/8b}$ have the same vacancy ratio, they have slightly different Young's moduli and ultimate tensile strengths. Another BNT couple, β_{12} and β_{13}, with the same vacancy ratio that is larger than the first couple (β_4 and $\eta_{1/8b}$) presents a larger discrepancy in terms of the aforementioned mechanical characteristics. The increase in the magnitude of discrepancy can be attributed to the increased configurational freedom of the BNTs as the vacancy ratio increases, which in turn amplifies the differences between the atomic arrangements affecting the mechanical behavior.

Using this similarity to nanoporous materials, we can deduce the following formulae for the determination of ultimate tensile strength and Youngs moduli:

$$\frac{\sigma^{ut}}{\sigma_0^{ut}} = \mathrm{C} \cdot \eta^{\mathrm{m}} \quad \textbf{(4.1)}$$

where σ^{ut} is the ultimate tensile stress of the nanoporous material, $\sigma_0{}^{ut}$ is the ultimate tensile stress of the non-porous material, C and m are the empirical constants of the power function determined from the curve in Figure 4.5, and η is the vacancy ratio.

Using values that we found from the results, we can deduce the formula for the ultimate tensile stress as

$$\frac{\sigma^{ut}}{708.2} = 0.1602 \cdot \eta^{-0.2669} \quad \textbf{(4.2)}$$

and similarly for the Young's moduli

$$\frac{E}{76.11} = 0.1036 \cdot \eta^{-0.3294} \quad \textbf{(4.3)}$$

at 300 K for the zigzag configurations. These formulae for the ultimate tensile stress and the Youngs moduli can be refined using results from a more diverse range of vacancy ratios.

Details of the mechanical behavior are discussed in the following subsections.

4.2.1 2-pmmn-Boron nanotubes

The 2-pmmn zigzag configuration has the highest fracture stress compared to all other structures investigated in this work. The unique structural strength of the 2-pmmn zigzag is an outcome of the bond formation. Bonds in 2-pmmn zigzag are laying in the direction of loading, thus providing structural support throughout the nanotube. Bond formations of the structure are given in Figure 4.6. As we can see from the figure, bonds in the tensile direction start breaking just before the failure and there are no defects in the nanotube to this point. Elongation is uniform across the nanotube.

The crack formation after the breakage of the longitudinal bonds was only observed at 1 K temperature. For higher temperatures, crack formation starts before the breakage of the first longitudinal bond break. This means there is almost no plastic deformation till rapture. Also, the ultimate tensile strain is much lower, as supposed to other structures we inspected. The sudden drop of the stress can be seen in Figure 4.9.

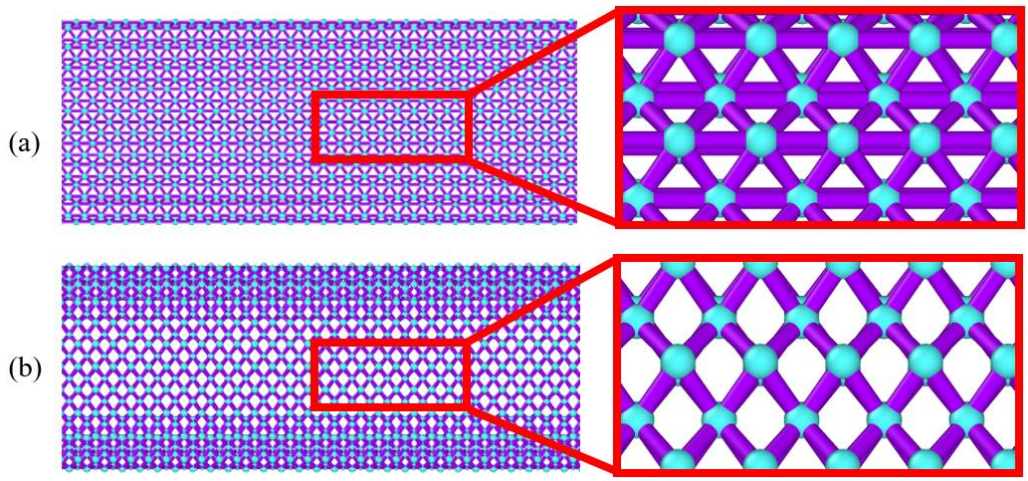

Figure 4.6 : Bond breakage for 2-pmmn zigzag structure. State of the bonds at (a) 11.12% and (b) 11.47% elongations.

Snapshots at the failure for the 2-pmmn zigzag structure are given in Figure 4.7. After the first crack formation, the stress path forms at a 45° angle to the loading direction. However, the direction of the crack growth is at 90° angle. There is almost no necking observed in the 2-pmmn zigzag.

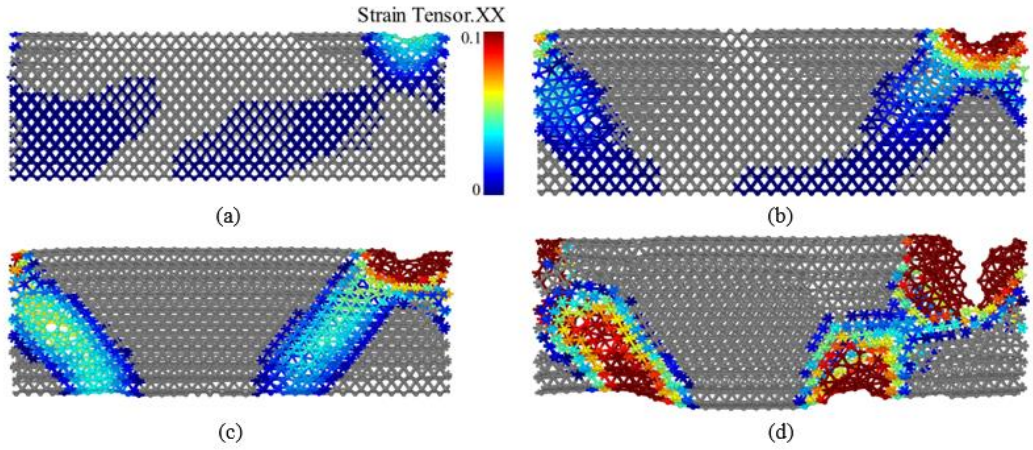

Figure 4.7 : Crack growth for 2-pmmn zigzag structure. Defect forms at 12.03% elongation (a) and rapidly grows at a 45-degree angle. Snapshots are at (b) 12.04%, (c) 12.05%, and (d) 12.15% elongations, respectively. Atoms and bonds are colored according to their respective strain level.

The 2-pmmn armchair has similar characteristics to its borophene counterpart. It has two different linear regimes like borophene as shown by Mortazavi et al.[40]. These two different regimes are a product of the process of out-of-plane atoms becoming in-plane. The non-homogeneous cross-section of the structure turns into a homogeneous

cross-section with a complex wavelike circle with all atoms in the tensile direction, which is given in Figure 4.8.

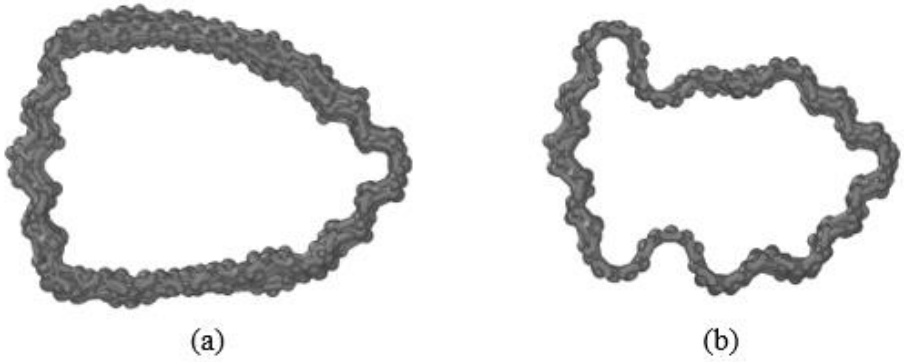

Figure 4.8 : Cross section of the 2-pmmn armchair; (a) at 10% elongation, (b) at 15% elongation.

The cross-section of the structure is not uniform after the thermalization. Potential energy per atom is also not homogeneous due to the shape of the cross-section. This rectangle-like shape has different bond energies across the cross-section owing to their distinct curvatures. Thus, high local potential energy gradients reduce the stability of the 2-pmmn armchair BNT structure and create a non-linear stress-strain curve. High potential energy gradient causes defect formation which in turn propagates to failure. In addition, the potential energy gradient increases with the temperature which consequently increases the strain gradient.

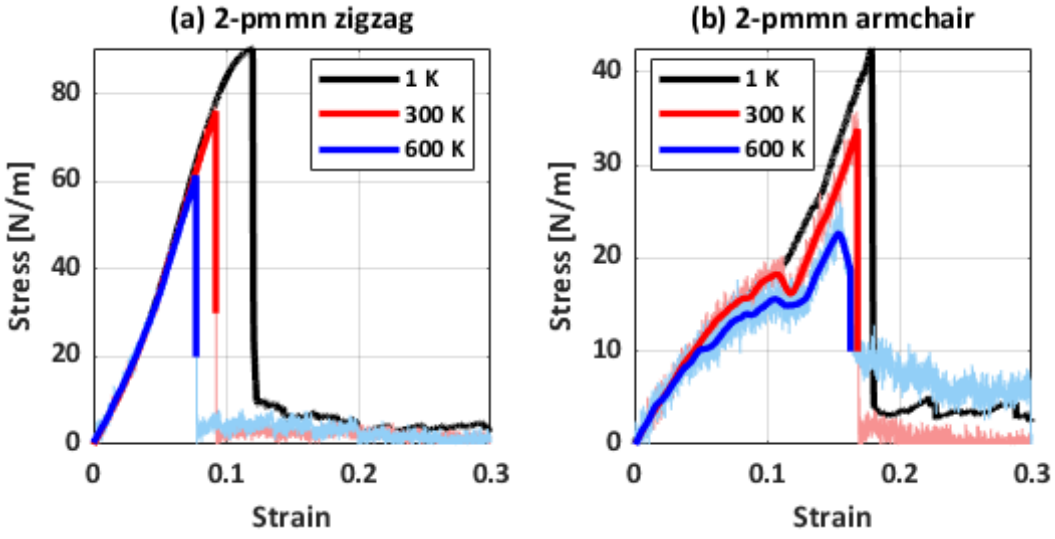

Figure 4.9 : Stress-strain curves of 2-pmmn (a) zigzag and (b) armchair configurations.

4.2.2 β-Boron nanotubes

In order to examine the interesting mechanical characteristics of β group BNT configurations, i.e. β_{12}, $\beta_{13,}$ β_4, and β_5, tensile stress-strain curves at different temperatures are provided in Figures 4.12, 4.13, 4.15, and 4.17, respectively. According to the curves, it is easily noticed that mechanical responses of the β type BNTs are significantly different, which clearly indicates the importance of the spatial arrangement of the atoms. Despite the equivalency of the vacancy ratios, β_{13} type BNT has much higher ductility compared to β_{12} structure. Simulation results also demonstrate that the β_4-BNT zigzag has the highest tensile strength and Young's modulus among the β structures. As another observation, it can be noted that armchair configurations generally have higher fracture strain compared to zigzag configurations owing to their bond angles. Unlike the bonds in the zigzag structure, the bonds in armchair structures are not oriented along the loading direction. Therefore, tensile deformation proceeds with the inclination of the bonds instead of elongation. As a result, they have higher ductility, which is in accordance with the DFT results reported by Kochaev [35].

In β structures, the spatial distribution of atomic potential energies is highly inhomogeneous at the unit cell level due to the diversity of the bond orders of the atoms. Yet, the potential energies of the atoms across the nanotube, given in Figure 4.10 :, repeat the same pattern with the unit cells. Thus, the structure can preserve the semi-circular cross-section.

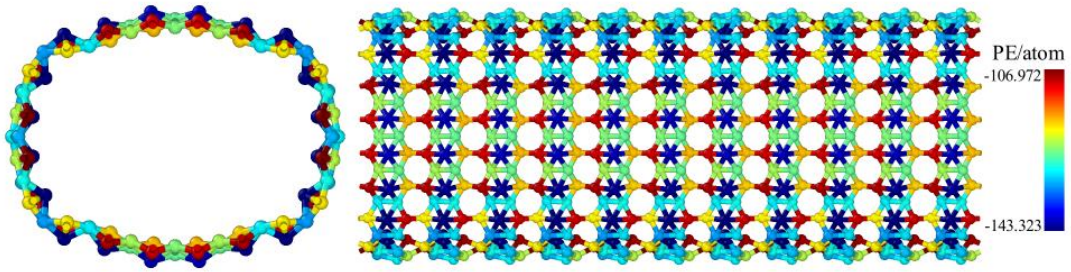

Figure 4.10 : Potential energy per atom for the β_{12}-BNT zigzag at 1 K.

β_{12}-BNT zigzag at 1 K possesses softening after around 12% elongations owing to continuous formation and breakage of the bonds. On the other hand, there is a breakage of around 100 bonds in the zigzag structure around 6-8% at 300 K, generating a flat section in the stress-strain curve during formation following a stiff response after

breakage ends. The bond breakage and contraction for the β_{12} zigzag BNT are given in Figure 4.11. The circled areas in Figure 4.11a and 4.11b shows the breaking bonds.

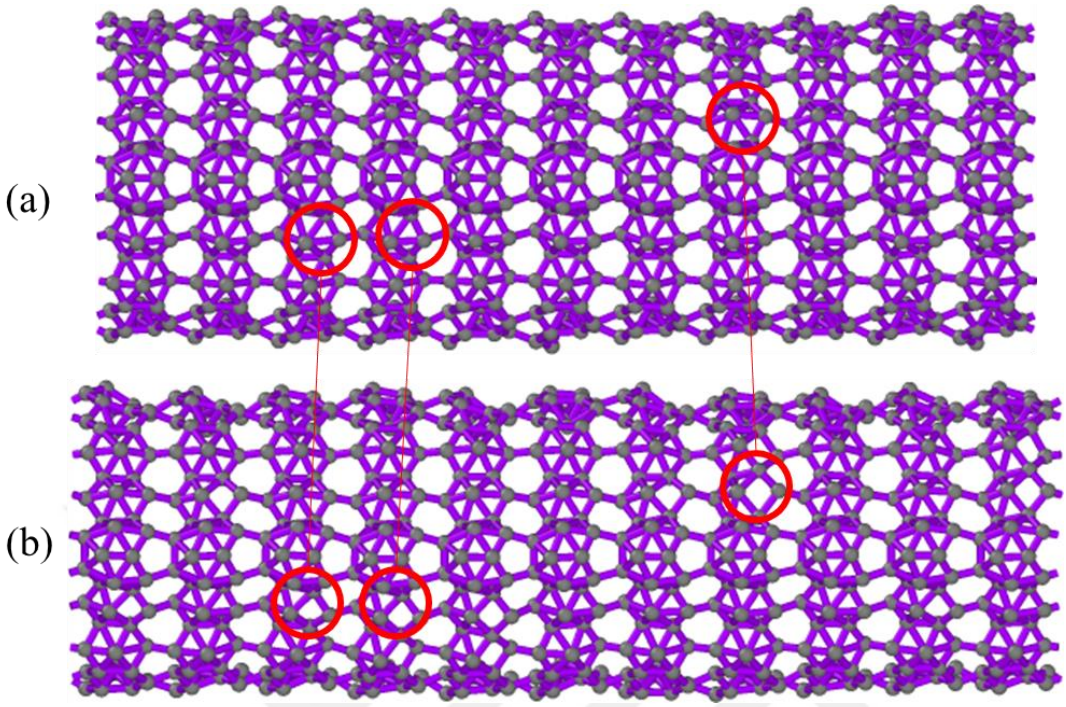

Figure 4.11 : State of bonds for β_{12} zigzag BNT at (a) 4% elongation and (b) at 7% elongation at 300 K.

The stable bonds at the two ends of the structure as given in Figure 4.3 : increase the stiffness of the structure. Yet, the structure is not able to maintain the uniform cross-section at 600 K due to high energy, thus can't form stable and uniform bonds which decreases the structural stability. The bond formation at 300 K creates a unique situation for the zigzag β_{12}-BNT, making them the only structure that has an increase of the strength with the temperature. β_{12}-BNT armchair at 1 K has sudden drops in the stress-strain curve due to the bond formation to collapse the structure.

We also observed stable bond formation in zigzag β_{13}-BNT at 300 K. Although, in zigzag β_{13}-BNT, formations start around 12% elongation and keep forming until fracture. Thus, stress levels can't increase while the strain increases.

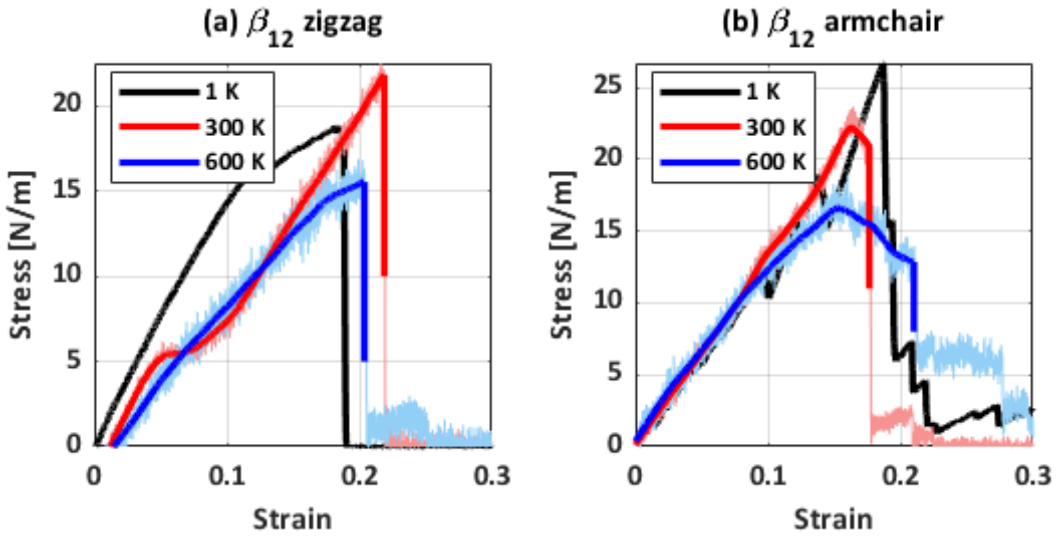

Figure 4.12 : Stress-strain curves of β_{12}-BNT, (a) zigzag (b) armchair.

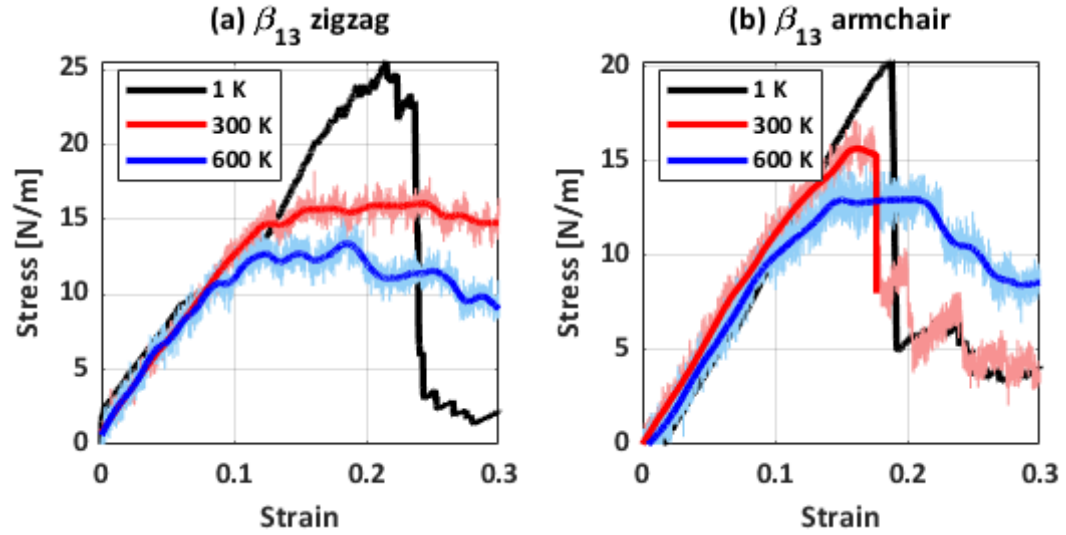

Figure 4.13 : Stress-strain curves of β_{13}-BNT, (a) zigzag (b) armchair.

For β_{13}-BNT, the stable forms are formed by contracting the nanotube. This is an outcome of the cross-section explained previously. As we can see from Figure 4.14, the bonds are forming across the nanotube which causes contraction and results in a ductile behavior. Since the bonds are not forming in the tensile direction, we can't observe the hardening behavior like β_{12}-BNT. The collapsing of the BNT is commonly observed in ductile behaving nanotubes.

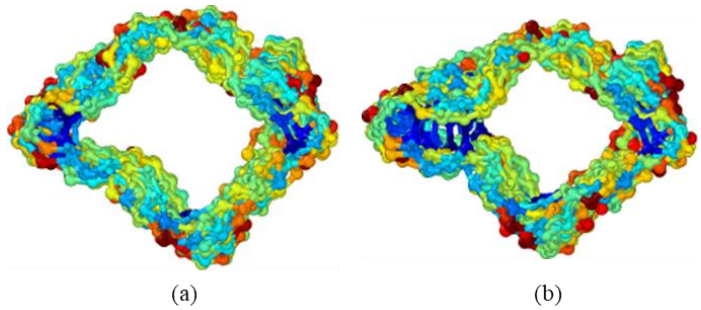

Figure 4.14 : Cross-section of β_{13}-BNT during tensile at 300 K. (a) at 12% elongation and (b) at 14% elongation.

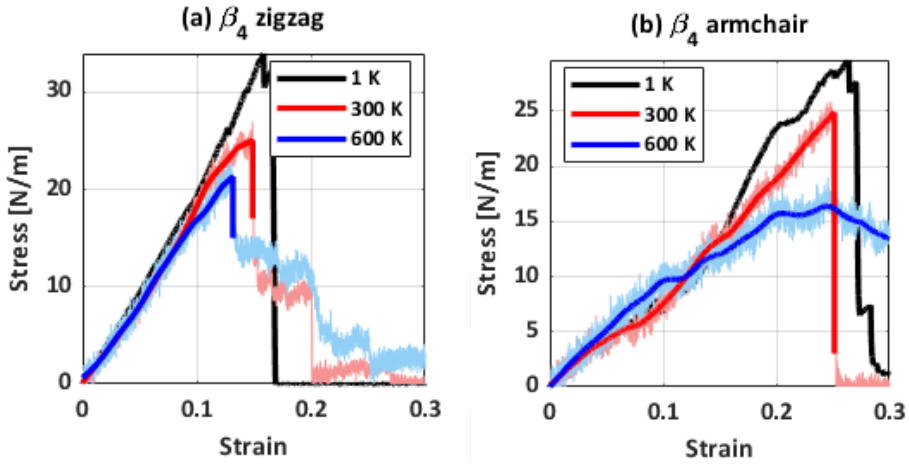

Figure 4.15 : Stress-strain curves of β_4-BNT, (a) zigzag (b) armchair.

β_4-BNT has the highest fracture stress among β structures. This is a consequence of the rectangle-like cross-section of the structure. The thickness of the cross-section slightly decreases with the increase in the elongation, but there are no bond formations like found on the β_{13}-BNT, so it doesn't collapse.

The behaviors of the β_4-BNT and β_5-BNTs are similar. The cross-section of the β_5-BNT at the beginning of the tensile process and 10% elongation is given in Figure 4.16. The semi-uniform cross-section does not collapse or contract like β_4-BNT.

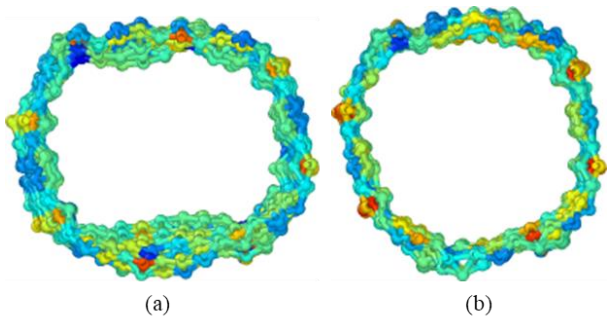

Figure 4.16 : The cross-section of the zigzag β_5-BNT at 300 K. (a) After the thermalization, (b) at 10% elongation.

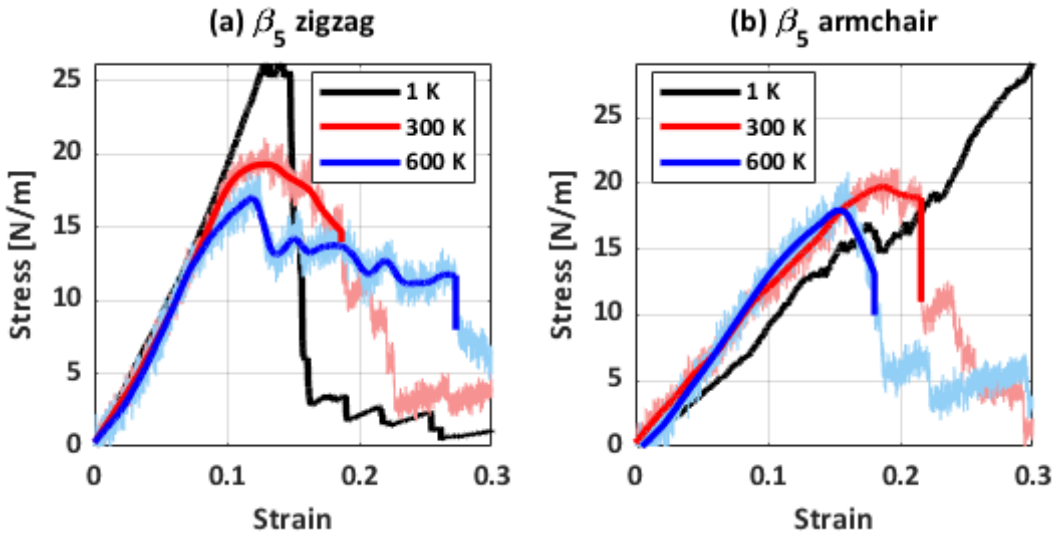

Figure 4.17 : Stress-strain curves of zigzag β_5-BNT, (a) zigzag (b) armchair

4.2.3 χ_3-Boron nanotubes

χ_3-BNT (Figure 4.18), has the highest ductility among other BNTs in the zigzag direction. Interestingly, ductility decreases in the armchair direction, unlike other BNTs. This property is a result of the hexagonal holes in the structure. The holes in the zigzag direction align axially in the nanotube in the zigzag direction, which reduces the strength of the material.

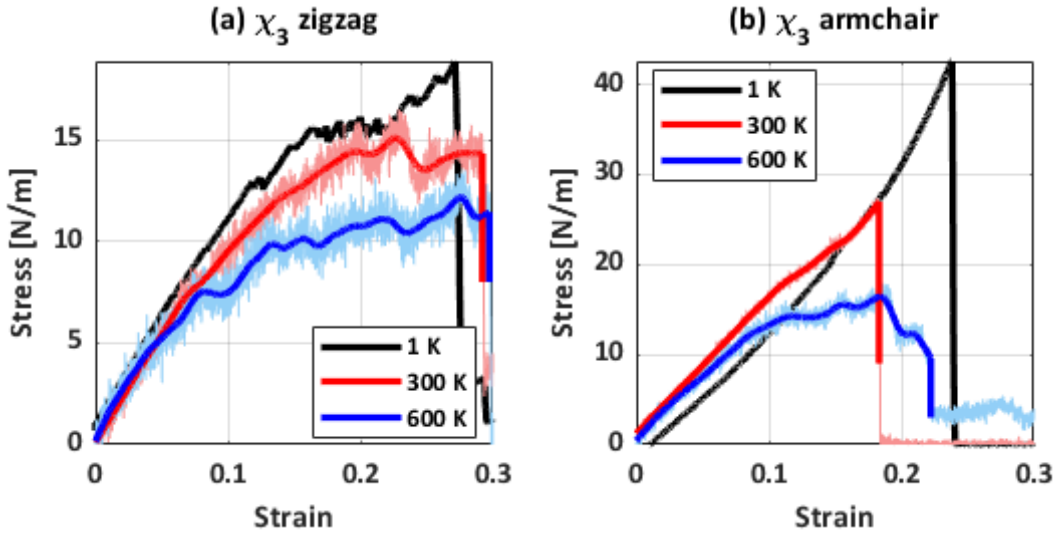

Figure 4.18 : Stress-strain curves of χ_3-BNT (a) zigzag (b) armchair

4.2.4 α-Boron nanotubes

Other BNTs have fairly strait stress-strain curves, indicating little to no bond formation during the tensile test. α-BNTs (Figure 4.19), regarded as the most stable by some a study [27], have one of the highest strengths in the zigzag direction and are very ductile

at the armchair direction. The ductility of the α-BNT increases with the temperature, while ultimate tensile strength decrease.

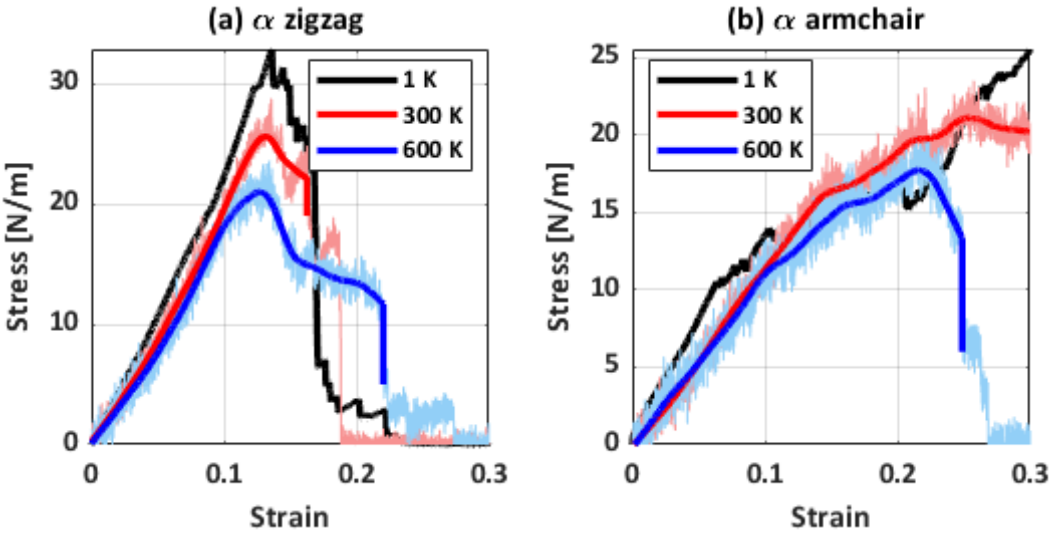

Figure 4.19 : Stress-strain curves of α-BNT, (a) zigzag (b) armchair.

4.2.5 δ_3-Boron nanotubes

δ_3-BNT, with a graphene-like hexagonal lattice, has the highest thermal stability. The structure has almost no noise in the stress-strain as can be seen in Figure 4.20. However, the structure is not stable in the armchair for the diameter we used in our work. Instability was also observed by Kunstmann et al. [26] in their DFT study for the distorted hexagonal BNT. They also reported that the 2-pmmn is also unstable yet we observed the opposite. The hexagonal structure might possess thermal stability for a larger diameter since the curvature will increase and the potential energy gradient will decrease. The stability of the hexagonal structure can be a topic for future studies.

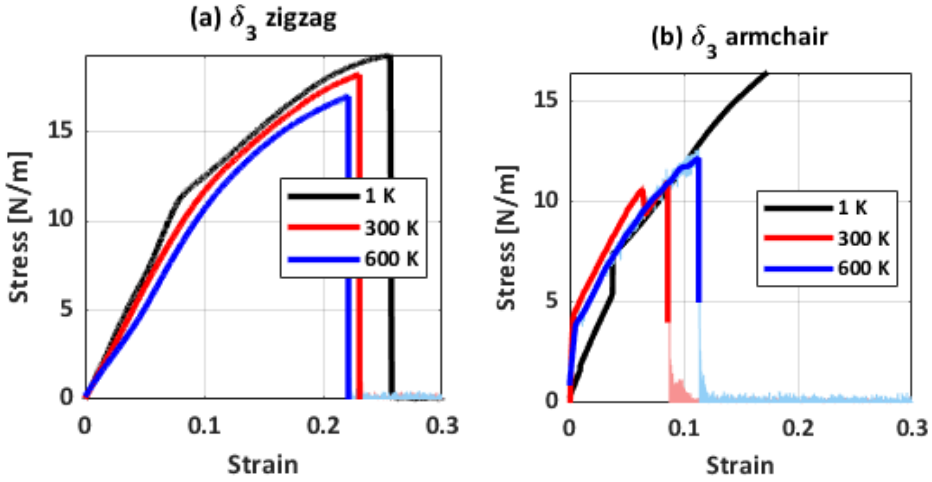

Figure 4.20 : Stress-strain curves of δ_3-BNT (a) zigzag (b) armchair.

4.2.6 Novel boron nanotubes

$\eta_{1/8b}$ and $\eta_{4/27}$ are proposed as an alternative BNT configuration for the first time in this study. We observed that they are thermally stable in 1, 300, and 600 K temperatures by using the molecular dynamics method. They have similar mechanical properties and structural characteristics to known configurations. The bond order of atoms in the lattice is different for every configuration, and low bond order atoms can be used as a bonding point for different atoms such as hydrogen for storage applications [71]. Although the mechanical strengths of the $\eta_{1/8b}$ and $\eta_{4/27}$ are not the best, every different vacancy ratio might possess useful properties in different applications.

Stress-strain curves for $\eta_{1/8b}$ and $\eta_{4/27}$ BNTs are given in Figures 4.21 and 4.22 respectively. The $\eta_{1/8b}$ has similar mechanical behavior to those seen in the β group as well as the $\eta_{4/27}$. The $\eta_{4/27}$-BNT has the highest isotropy among BNTs, meaning the armchair and the zigzag configurations have very similar structural properties.

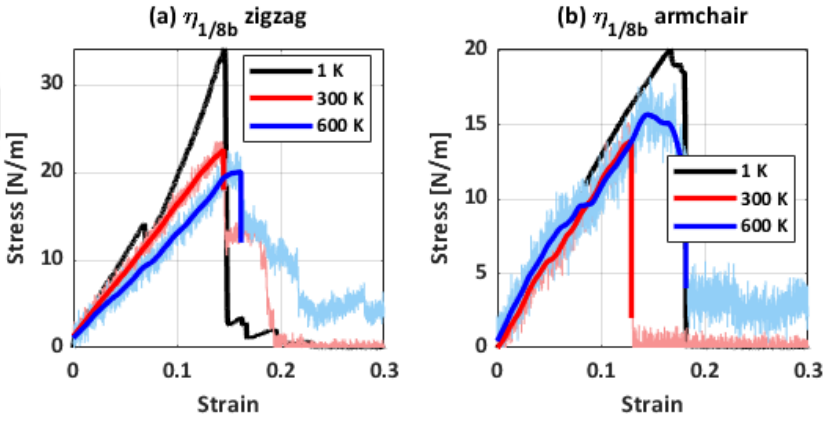

Figure 4.21 : Stress-strain curves of $\eta_{1/8b}$-BNT (a) zigzag (b) armchair.

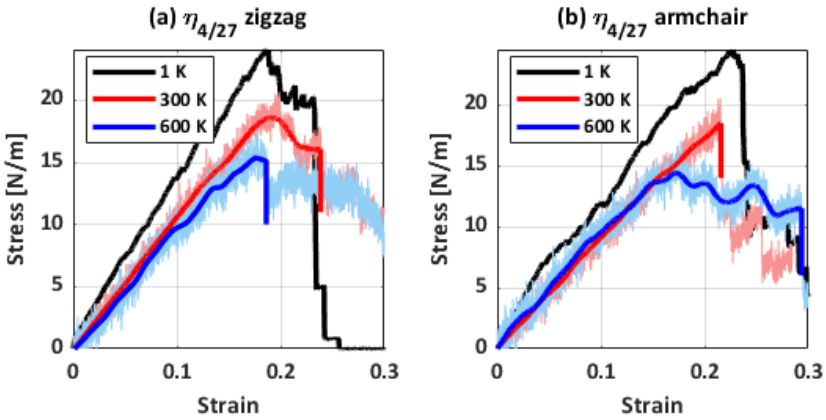

Figure 4.22 : Stress-strain curves of $\eta_{4/27}$ -BNT (a) zigzag (b) armchair.

5. CONCLUSION AND RECOMMENDATIONS

In conclusion, we outlined a novel method to examine the properties of BNTs. We reveal that the reactive molecular dynamics can successfully model unique aspects of the BNTs and can be utilized to investigate mechanical properties.

We observed that the ReaxFF force field can successfully minimize the energy of the BNTs. It can also model the thermal equilibrium with the structural properties spotted in quantum mechanics simulations such as surface buckling and elliptic shape. Our results indicate that the BNTs around 1.7 nm diameter are thermally stable, except δ_3 at 1.61 nm diameter, which is coherent with the DFT simulations. We also noted that the lattice parameters change similar to those seen in borophene. Although this effect doesn't influence the mechanical properties.

Mechanical properties of BNTs were found to be highly dependent on their vacancy ratio, atomic configuration, and chirality. Also, BNTs exhibit highly anisotropic behavior. Young moduli and ultimate tensile stress of nanotubes are generally two times higher in the zigzag direction, yet the ultimate tensile strain is two times higher in the armchair direction, except for some configurations explained in the previous chapter.

Stiffness and strength in general decrease while the vacancy ratio and temperature increase. The potential energy difference per atom due to the bond order is the root cause of the defect formation. Some structures exhibit plastic behavior owing to stable bond formations during tensile.

Our results depict that the 2-pmmn zigzag BNT has the highest ultimate tensile stress and Young's modulus. In addition, χ_3 armchair, α armchair, and α zigzag have the highest ultimate tensile stress, strain, and Young's modulus among planar structures, respectively. Ultimate tensile stress and stiffness of the structures generally decrease while the vacancy ratio and temperature increase.

Thermally stable BNTs can be great analogs for other nanotubes such as CNTs and BNNTs due to their metallic behavior. Furthermore, their vacancies can be exploited

for several applications such as hydrogen storage. Thermal properties, nanocomposites with BNTs can be subject to future studies.

REFERENCES

[1] **Iijima, S.** (1991). Helical microtubules of graphitic carbon. *Nature*, Nature Publishing Group. 354, 56–8. https://doi.org/10.1038/354056a0

[2] **Geim, A.K. and Novoselov, K.S.** (2007). The rise of graphene. *Nature Materials*, 6, 183–91. https://doi.org/10.1038/nmat1849

[3] **Feng, B., Zhang, J., Liu, R.Y., Iimori, T., Lian, C., Li, H. et al.** (2016). Direct evidence of metallic bands in a monolayer boron sheet. *Physical Review B*, American Physical Society. 94, 041408. https://doi.org/10.1103/PhysRevB.94.041408

[4] **Vogt, P., De Padova, P., Quaresima, C., Avila, J., Frantzeskakis, E., Asensio, M.C. et al.** (2012). Silicene: Compelling experimental evidence for graphenelike two-dimensional silicon. *Physical Review Letters*, American Physical Society. 108, 155501. https://doi.org/10.1103/PhysRevLett.108.155501

[5] **Feng, B., Ding, Z., Meng, S., Yao, Y., He, X., Cheng, P. et al.** (2012). Evidence of silicene in honeycomb structures of silicon on Ag(111). *Nano Letters*, American Chemical Society. 12, 3507–11. https://doi.org/10.1021/nl301047g

[6] **Dávila, M.E., Xian, L., Cahangirov, S., Rubio, A. and Le Lay, G.** (2014). Germanene: A novel two-dimensional germanium allotrope akin to graphene and silicene. *New Journal of Physics*, IOP Publishing. 16, 095002. https://doi.org/10.1088/1367-2630/16/9/095002

[7] **Li, L., Lu, S.Z., Pan, J., Qin, Z., Wang, Y.Q., Wang, Y. et al.** (2014). Buckled germanene formation on Pt(111). *Advanced Materials*, John Wiley & Sons, Ltd. 26, 4820–4. https://doi.org/10.1002/adma.201400909

[8] **Mannix, A.J., Zhou, X.F., Kiraly, B., Wood, J.D., Alducin, D., Myers, B.D. et al.** (2015). Synthesis of borophenes: Anisotropic, two-dimensional boron polymorphs. *Science*, American Association for the Advancement of Science. 350, 1513–6. https://doi.org/10.1126/science.aad1080

[9] **Feng, B., Zhang, J., Zhong, Q., Li, W., Li, S., Li, H. et al.** (2016). Experimental realization of two-dimensional boron sheets. *Nature Chemistry*, Nature Publishing Group. 8, 563–8. https://doi.org/10.1038/nchem.2491

[10] **Sands, D.E. and Hoard, J.L.** (1957). Rhombohedral elemental boron [Internet]. J. Am. Chem. Soc. American Chemical Society. p. 5582–3. https://doi.org/10.1021/ja01577a072

[11] **Woods, W.G.** (1994). An introduction to boron: History, sources, uses, and chemistry. *Environmental Health Perspectives*, Public Health Services, US Dept of Health and Human Services. p. 5–11. https://doi.org/10.1289/ehp.94102s75

[12] **Ogitsu, T., Schwegler, E. and Galli, G.** (May 8, 2013). β-Rhombohedral boron: At the crossroads of the chemistry of boron and the physics of frustration [Internet]. Chem. Rev. American Chemical Society. p. 3425–49. https://doi.org/10.1021/cr300356t

[13] **Tian, J., Xu, Z., Shen, C., Liu, F., Xu, N. and Gao, H.J.** (2010). One-dimensional boron nanostructures: Prediction, synthesis, characterizations, and applications. *Nanoscale*, The Royal Society of Chemistry. 2, 1375–89. https://doi.org/10.1039/c0nr00051e

[14] **Boustani, I. and Quandt, A.** (1997). Nanotubules of bare boron clusters: Ab initio and density functional study. *Europhysics Letters*, IOP Publishing. 39, 527–32. https://doi.org/10.1209/epl/i1997-00388-9

[15] **Ciuparu, D., Klie, R.F., Zhu, Y. and Pfefferle, L.** (2004). Synthesis of Pure Boron Single-Wall Nanotubes. *Journal of Physical Chemistry B*, American Chemical Society. 108, 3967–9. https://doi.org/10.1021/jp049301b

[16] **Liu, F., Shen, C., Su, Z., Ding, X., Deng, S., Chen, J. et al.** (2010). Metal-like single crystalline boron nanotubes: Synthesis and in situ study on electric transport and field emission properties. *Journal of Materials Chemistry*, The Royal Society of Chemistry. 20, 2197–205. https://doi.org/10.1039/b919260c

[17] **Liu, J. and Iqbal, Z.** (2011). Facile synthesis of pure boron nanotubes and nanofibers. *Materials Research Society Symposium Proceedings*, Cambridge University Press. 1307, 42–7. https://doi.org/10.1557/opl.2011.320

[18] **Wildöer, J.W.G., Venema, L.C., Rinzler, A.G., Smalley, R.E. and Dekker, C.** (1998). Electronic structure of atomically resolved carbon nanotubes. *Nature*, Nature Publishing Group. 391, 59–62. https://doi.org/10.1038/34139

[19] **Odom, T.W., Huang, J.L., Kim, P. and Lieber, C.M.** (1998). Atomic structure and electronic properties of single-walled carbon nanotubes. *Nature*, Nature Publishing Group. 391, 62–4. https://doi.org/10.1038/34145

[20] **Sebetci, A., Mete, E. and Boustani, I.** (2008). Free standing double walled boron nanotubes. *Journal of Physics and Chemistry of Solids*, Pergamon. 69, 2004–12. https://doi.org/10.1016/j.jpcs.2008.02.014

[21] **Singh, A.K., Sadrzadeh, A. and Yakobson, B.I.** (2008). Probing properties of boron a-tubes by Ab Initio calculations. *Nano Letters*, American Chemical Society. 8, 1314–7. https://doi.org/10.1021/nl073295o

[22] **Yang, X., Ding, Y. and Ni, J.** (2008). Ab initio prediction of stable boron sheets and boron nanotubes: Structure, stability, and electronic properties. *Physical Review B - Condensed Matter and Materials Physics*, American Physical Society. 77, 041402. https://doi.org/10.1103/PhysRevB.77.041402

[23] **Tang, H. and Ismail-Beigi, S.** (2010). First-principles study of boron sheets and nanotubes. *Physical Review B - Condensed Matter and Materials Physics*, 82, 1–20. https://doi.org/10.1103/PhysRevB.82.115412

[24] **Szwacki, N.G. and Tymczak, C.J.** (2010). The symmetry of the boron buckyball and a related boron nanotube. *Chemical Physics Letters*, Elsevier B.V. 494, 80–3. https://doi.org/10.1016/j.cplett.2010.05.086

[25] **Gunasinghe, R.N., Kah, C.B., Quarles, K.D. and Wang, X.Q.** (2011). Dispersion corrections in the boron buckyball and nanotubes. *Applied Physics*

Letters, American Institute of PhysicsAIP. 98, 261906. https://doi.org/10.1063/1.3604018

[26] **Kunstmann, J., Bezugly, V., Rabbel, H., Rümmeli, M.H. and Cuniberti, G.** (2014). Unveiling the atomic structure of single-wall boron nanotubes. *Advanced Functional Materials*, 24, 4127–34. https://doi.org/10.1002/adfm.201304146

[27] **Bezugly, V., Kunstmann, J., Grundkötter-Stock, B., Frauenheim, T., Niehaus, T. and Cuniberti, G.** (2011). Highly conductive boron nanotubes: Transport properties, work functions, and structural stabilities. *ACS Nano*, American Chemical Society. 5, 4997–5005. https://doi.org/10.1021/nn201099a

[28] **Wu, S., Yang, Z., Guo, A.M. and Ouyang, F.** (2021). Electron transport along boron nanotubes rolled from β12-borophene: A first-principles study. *Physica E: Low-Dimensional Systems and Nanostructures*, Elsevier B.V. 126, 114457. https://doi.org/10.1016/j.physe.2020.114457

[29] **Ding, Y. and Ni, J.** (2009). Electronic properties of boron nanotubes with axial strain. *Frontiers of Physics in China*, Springer. 4, 383–8. https://doi.org/10.1007/s11467-009-0028-4

[30] **Le, M.Q., Mortazavi, B. and Rabczuk, T.** (2016). Mechanical properties of borophene films: A reactive molecular dynamics investigation. *Nanotechnology*, Institute of Physics Publishing. 27. https://doi.org/10.1088/0957-4484/27/44/445709

[31] **Tang, H. and Ismail-Beigi, S.** (2007). Novel precursors for boron nanotubes: The competition of two-center and three-center bonding in boron sheets. *Physical Review Letters*, American Physical Society. 99, 115501. https://doi.org/10.1103/PhysRevLett.99.115501

[32] **Kunstmann, J. and Quandt, A.** (2005). Constricted boron nanotubes. *Chemical Physics Letters*, 402, 21–6. https://doi.org/10.1016/j.cplett.2004.11.130

[33] **Kunstmann, J. and Quandt, A.** (2006). Broad boron sheets and boron nanotubes: An ab initio study of structural, electronic, and mechanical properties. *Physical Review B - Condensed Matter and Materials Physics*, American Physical Society. 74, 035413. https://doi.org/10.1103/PhysRevB.74.035413

[34] **Evans, M.H., Joannopoulos, J.D. and Pantelides, S.T.** (2005). Electronic and mechanical properties of planar and tubular boron structures. *Physical Review B - Condensed Matter and Materials Physics*, 72. https://doi.org/10.1103/PhysRevB.72.045434

[35] **Kochaev, A.** (2017). Elastic properties of noncarbon nanotubes as compared to carbon nanotubes. *Physical Review B*, 96, 1–7. https://doi.org/10.1103/PhysRevB.96.155428

[36] **Zhang, J. and Zhou, J.** (2021). Buckling of boron nanotubes under axial compression: Insights from molecular mechanics and continuum mechanics. *Physica E: Low-Dimensional Systems and Nanostructures*, Elsevier B.V. 127, 114520. https://doi.org/10.1016/j.physe.2020.114520

[37] **Aziz, B., Asha, A.S. and Ali, M.A.** (2021). Evaluation of mechanical properties of borophene nanotube by molecular dynamics simulation. *AIP Conference Proceedings*, AIP Publishing LLC AIP Publishing. 2324, 030022. https://doi.org/10.1063/5.0037898

[38] **Zhou, Y.P. and Jiang, J.W.** (2017). Molecular dynamics simulations for mechanical properties of borophene: Parameterization of valence force field model and Stillinger-Weber potential. *Scientific Reports*, Nature Publishing Group. 7, 1–12. https://doi.org/10.1038/srep45516

[39] **Mortazavi, B., Rahaman, O., Dianat, A. and Rabczuk, T.** (2016). Mechanical responses of borophene sheets: A first-principles study. *Physical Chemistry Chemical Physics*, Royal Society of Chemistry. 18, 27405–13. https://doi.org/10.1039/c6cp03828j

[40] **Mortazavi, B., Le, M.Q., Rabczuk, T. and Pereira, L.F.C.** (2017). Anomalous strain effect on the thermal conductivity of borophene: a reactive molecular dynamics study. *Physica E: Low-Dimensional Systems and Nanostructures*, North-Holland. 93, 202–7. https://doi.org/10.1016/j.physe.2017.06.012

[41] **Sadeghzadeh, S.** (2018). Borophene sheets with in-plane chain-like boundaries; a reactive molecular dynamics study. *Computational Materials Science*, Elsevier B.V. 143, 1–14. https://doi.org/10.1016/j.commatsci.2017.10.047

[42] **Sadeghzadeh, S. and Khatibi, M.M.** (2018). Vibrational modes and frequencies of borophene in comparison with graphene nanosheets. *Superlattices and Microstructures*, Academic Press. 117, 271–82. https://doi.org/10.1016/J.SPMI.2018.03.059

[43] **Arabha, S., Akbarzadeh, A.H. and Rajabpour, A.** (2020). Engineered porous borophene with tunable anisotropic properties. *Composites Part B: Engineering*, Elsevier. 200, 108260. https://doi.org/10.1016/J.COMPOSITESB.2020.108260

[44] **Frenkel, D. and Smit, B.** (2002). Understanding Molecular Simulation (Second Edition) [Internet]. Frenkel D, and Smit B, editors. Underst. Mol. Simul. (Second Ed. Academic Press.

[45] **Braun, E., Gilmer, J., Mayes, H.B., Mobley, D.L., Monroe, J.I., Prasad, S. et al.** (2019). Best Practices for Foundations in Molecular Simulations [Article v1.0]. *Living Journal of Computational Molecular Science*, University of Colorado at Boulder. 1, 5957–5957. https://doi.org/10.33011/LIVECOMS.1.1.5957

[46] **Senftle, T.P., Hong, S., Islam, M.M., Kylasa, S.B., Zheng, Y., Shin, Y.K. et al.** (2016). The ReaxFF reactive force-field: Development, applications and future directions. *Npj Computational Materials*, 2. https://doi.org/10.1038/npjcompumats.2015.11

[47] **Daw, M.S. and Baskes, M.I.** (1984). Embedded-atom method: Derivation and application to impurities, surfaces, and other defects in metals. *Physical Review B*, American Physical Society. 29, 6443. https://doi.org/10.1103/PhysRevB.29.6443

[48] **Baskes, M.I.** (1992). Modified embedded-atom potentials for cubic materials

and impurities. *Physical Review B*, American Physical Society. 46, 2727. https://doi.org/10.1103/PhysRevB.46.2727

[49] **Stillinger, F.H. and Weber, T.A.** (1985). Computer simulation of local order in condensed phases of silicon. *Physical Review B*, American Physical Society. 31, 5262. https://doi.org/10.1103/PhysRevB.31.5262

[50] **A. D. MacKerell, J., Bashford, D., Bellott, M., R. L. Dunbrack, J., Evanseck, J.D., Field, M.J. et al.** (1998). All-Atom Empirical Potential for Molecular Modeling and Dynamics Studies of Proteins †. *Journal of Physical Chemistry B*, American Chemical Society. 102, 3586–616. https://doi.org/10.1021/JP973084F

[51] **Cornell, W.D., Cieplak, P., Bayly, C.I., Gould, I.R., Merz, K.M., Ferguson, D.M. et al.** (2002). A Second Generation Force Field for the Simulation of Proteins, Nucleic Acids, and Organic Molecules. *Journal of the American Chemical Society*, American Chemical Society. 117, 5179–97. https://doi.org/10.1021/JA00124A002

[52] **Rappe, A.K., Casewit, C.J., Colwell, K.S., III, W.A.G. and Skiff, W.M.** (2002). UFF, a full periodic table force field for molecular mechanics and molecular dynamics simulations. *Journal of the American Chemical Society*, American Chemical Society. 114, 10024–35. https://doi.org/10.1021/JA00051A040

[53] **Mayo, S.L., Olafson, B.D. and Goddard, W.A.** (2002). DREIDING: a generic force field for molecular simulations. *Journal of Physical Chemistry*, American Chemical Society . 94, 8897–909. https://doi.org/10.1021/J100389A010

[54] **Stuart, S.J., Tutein, A.B. and Harrison, J.A.** (2000). A reactive potential for hydrocarbons with intermolecular interactions. *The Journal of Chemical Physics*, American Institute of PhysicsAIP. 112, 6472. https://doi.org/10.1063/1.481208

[55] **Brenner, D.W., Shenderova, O.A., Harrison, J.A., Stuart, S.J., Ni, B., Sinnott, S.B. et al.** (2002). A second-generation reactive empirical bond order (REBO) potential energy expression for hydrocarbons. *JPCM*, 14, 783–802. https://doi.org/10.1088/0953-8984/14/4/312

[56] **Orekhov, N., Ostroumova, G. and Stegailov, V.** (2020). High temperature pure carbon nanoparticle formation: Validation of AIREBO and ReaxFF reactive molecular dynamics. *Carbon*, Pergamon. 170, 606–20. https://doi.org/10.1016/J.CARBON.2020.08.009

[57] **Chenoweth, K., Van Duin, A.C.T. and Goddard, W.A.** (2008). ReaxFF reactive force field for molecular dynamics simulations of hydrocarbon oxidation. *Journal of Physical Chemistry A*, American Chemical Society . 112, 1040–53. https://doi.org/10.1021/jp709896w

[58] **Van Duin, A.C.T., Dasgupta, S., Lorant, F. and Goddard, W.A.** (2001). ReaxFF: A reactive force field for hydrocarbons. *Journal of Physical Chemistry A*, 105, 9396–409. https://doi.org/10.1021/jp004368u

[59] **Pai, S.J., Yeo, B.C. and Han, S.S.** (2016). Development of the ReaxFFCBN reactive force field for the improved design of liquid CBN hydrogen storage materials. *Physical Chemistry Chemical Physics*, Royal Society of Chemistry.

18, 1818–27. https://doi.org/10.1039/c5cp05486a

[60] **Wang, H., Li, Q., Gao, Y., Miao, F., Zhou, X.F. and Wan, X.G.** (2016). Strain effects on borophene: Ideal strength, negative Possion's ratio and phonon instability. *New Journal of Physics*, IOP Publishing. 18. https://doi.org/10.1088/1367-2630/18/7/073016

[61] **Zhang, X., Hu, J., Cheng, Y., Yang, H.Y., Yao, Y. and Yang, S.A.** (2016). Borophene as an extremely high capacity electrode material for Li-ion and Na-ion batteries. *Nanoscale*, 8, 15340–7. https://doi.org/10.1039/c6nr04186h

[62] **Plimpton, S.** (1995). Fast parallel algorithms for short-range molecular dynamics. *Journal of Computational Physics*, Academic Press. 117, 1–19. https://doi.org/10.1006/jcph.1995.1039

[63] **Aktulga, H.M., Fogarty, J.C., Pandit, S.A. and Grama, A.Y.** (2012). Parallel reactive molecular dynamics: Numerical methods and algorithmic techniques. *Parallel Computing*, North-Holland. 38, 245–59. https://doi.org/10.1016/J.PARCO.2011.08.005

[64] **Aktulga, H.M., Knight, C., Coffman, P., O'Hearn, K.A., Shan, T.R. and Jiang, W.** (2019). Optimizing the performance of reactive molecular dynamics simulations for many-core architectures. *International Journal of High Performance Computing Applications*, SAGE Publications Inc. 33, 304–21. https://doi.org/10.1177/1094342017746221

[65] **Polak, E. and Ribiere, G.** (1969). Note sur la convergence de méthodes de directions conjuguées. *ESAIM: Mathematical Modelling and Numerical Analysis - Modélisation Mathématique et Analyse Numérique*, 3, 35–43.

[66] min_style command — LAMMPS documentation [Internet].

[67] **Wu, R., Drozdov, I.K., Eltinge, S., Zahl, P., Ismail-Beigi, S., Božović, I. et al.** (2019). Large-area single-crystal sheets of borophene on Cu(111) surfaces. *Nature Nanotechnology*, Nature Publishing Group. 14, 44–9. https://doi.org/10.1038/s41565-018-0317-6

[68] **Mazaheri, A., Javadi, M. and Abdi, Y.** (2021). Chemical vapor deposition of two-dimensional boron sheets by thermal decomposition of diborane. *ACS Applied Materials and Interfaces*, 13, 8844–50. https://doi.org/10.1021/acsami.0c22580

[69] **Chahal, S., Ranjan, P., Motlag, M., Yamijala, S.S.R.K.C., Late, D.J., Sadki, E.H.S. et al.** (2021). Borophene via Micromechanical Exfoliation. *Advanced Materials*,. https://doi.org/10.1002/adma.202102039

[70] **Yazdani, H., Hatami, K. and Eftekhari, M.** (2017). Mechanical properties of single-walled carbon nanotubes: a comprehensive molecular dynamics study. *Materials Research Express*, IOP Publishing. 4, 055015. https://doi.org/10.1088/2053-1591/AA7003

[71] **Li, F., Wei, W., Sun, Q., Yu, L., Huang, B. and Dai, Y.** (2017). Prediction of Single-Wall Boron Nanotube Structures and the Effects of Hydrogenation. https://doi.org/10.1021/acs.jpcc.7b00554

APPENDICES

APPENDIX A: Scripts

APPENDIX A1: Sample Matlab code for BNT generation

```
clear all

maxneigh = 6;
bigspace = 100.0;

lenxyz = zeros(3,1);
shift0 = zeros(3,1);
shift = zeros(3,1);

ltube = false;
nlayer = 1;

u_vec = 60;
v_vec = 60;
S = [1];

for u = 1:length(u_vec)
    for v = 1:length(v_vec)
        natomcell = 4;
        lenxyz(1) = v_vec(v);
        lenxyz(2) = u_vec(u);

        wl1 = lenxyz(1);
        wl2 = lenxyz(2);

        %data from New J. Phys. 18, 073016 (2016)
        a2 = 1/2 * 2.866;
        a1 = 1/2 * 1.614;
        a3 = 20.0;
        h = 0.911;
        thicknessiner = h;

        coord(1,1) = 0;
        coord(2,1) = 0;
        coord(3,1) = 0;
        coord(1,2) = 1 * a1;
```

```
        coord(2,2) = 1 * a2;
        coord(3,2) = h;
        coord(1,3) = 2 * a1;
        coord(2,3) = 0;
        coord(3,3) = 0;
        coord(1,4) = 3 * a1;
        coord(2,4) = 1 * a2;
        coord(3,4) = h;

        box_x = 4 * a1;
        box_y = 2 * a2;
        box_z = a3;
        shift0(2) = a2;

        nx = lenxyz(1)/box_x;
        nx = floor(nx);
        lenxyz(1) = nx * box_x;
        ny = lenxyz(2)/box_y;
        ny = floor(ny);
        lenxyz(2) = ny * box_y;
        nz = nlayer;
        lenxyz(3) = nz * box_z;

        N = natomcell * nx * ny * nz;
        N = round(N);
        ntot = N;

        for iz = 1:nz
            z0 = real(iz-1) * box_z;
            shift(:) = shift0(:) *real(mod(iz-1,2));
            for i = 1:nx
                for j = 1:ny
                    x0 = (i-1) * box_x;
                    y0 = (j-1) * box_y;
                    k=(iz-1)*nx*ny*natomcell+(i-1)*ny*natomcell+...
(j-1)*natomcell;
                    for ii = 1: natomcell
                        k = k + 1;
                        xalat(k) = x0 + coord(1,ii) + shift(1);
                        yalat(k) = y0 + coord(2,ii) + shift(2);
                        zalat(k) = z0 + coord(3,ii) + shift(3);
                        atnum(k) = 5;
                        atype(k) = ii;
                    end
                end
            end
        end

        diameter = lenxyz(2)/pi();
```

```
        if ltube
            radius = 0.5*diameter - 0.5*thicknessiner;
            ly = pi * diameter;
            for i = 1:2:k %round(k)
                theta = 2.0*pi()*yalat(i)/ly;
                xalat(i) = xalat(i);
                yalat(i) = radius * cos(theta);
                zalat(i) = radius * sin(theta);
            end
            radius = 0.5*diameter + 0.5*thicknessiner;
            ly = pi * diameter;
            for i = 2:2:round(k)
                theta = 2.0*pi()*yalat(i)/ly;
                xalat(i) = xalat(i);
                yalat(i) = radius * cos(theta);
                zalat(i) = radius * sin(theta);
            end
        end

        mdbox(:) = lenxyz(:);

        if ltube
            mdbox(2) = mdbox(2) + bigspace;
            mdbox(3) = mdbox(3) + bigspace;
        else
            mdbox(3) = mdbox(3) + bigspace;
        end

        if ltube
            for i = 1:k
                yalat(i) = yalat(i) + 0.5 * mdbox(2);
                zalat(i) = zalat(i) + 0.5 * mdbox(3);
            end
        else
            for i = 1:k
                zalat(i) = zalat(i) + 0.5 * mdbox(3);
            end
        end

        coordinates = [transpose(xalat) transpose(yalat)...
transpose(zalat)];

        xlo = min(coordinates(:,1)) - 1/2 * a1;
        xhi = max(coordinates(:,1)) + 1/2 * a1;

        d1 = max(coordinates(:,2));
        d2 = min(coordinates(:,2));
        diameter = (abs(d1)-abs(d2))/10 - h/20
```

```
        r = diameter/2

        l1 = max(coordinates(:,1));
        l2 = min(coordinates(:,1));
        lng = (abs(l1)-abs(l2))/10;

        aspectratio = lng/r

        if ltube
            ylo = min(coordinates(:,2)) -50;
            yhi = max(coordinates(:,2)) +50;
            zlo = min(coordinates(:,3)) -50;
            zhi = max(coordinates(:,3)) +50;
        else
            ylo = min(coordinates(:,2)) -1/2 * a2;
            yhi = max(coordinates(:,2)) +1/2 * a2;
            zlo = min(coordinates(:,3)) -50;
            zhi = max(coordinates(:,3)) +50;
        end

        filename=['T',num2str(S),'.',num2str(wl2),'x',num2str(wl1),'.',
num2str(ltube),'.lammpsdata'];
        fid=fopen(filename,'w');
        leng=length(coordinates(:,1));
        Out1=[num2str(leng),' atoms\n'];
        Out2=[num2str(xlo),' ',num2str(xhi),' xlo xhi\n'];
        Out3=[num2str(ylo),' ',num2str(yhi),' ylo yhi\n'];
        Out4=[num2str(zlo),' ',num2str(zhi),' zlo zhi\n'];
        Out5=[num2str(1),' atom types\n'];
        Out6=['# LAMMPS data file for armchair T',num2str(S), ...
            ' diameter:',num2str(diameter), ' length:',num2str(lng), '
aspect ratio:',num2str(aspectratio),'\n'];
        fprintf(fid,Out6);
        fprintf(fid,Out1);
        fprintf(fid,Out5);
        fprintf(fid,Out2);
        fprintf(fid,Out3);
        fprintf(fid,Out4);
        fprintf(fid,'\n');
        fprintf(fid,'Atoms\n');
        fprintf(fid,'\n');
        for j=1:1:ntot
            fprintf(fid,'%d %d %d %12.6f %12.6f %12.6f\n', j, 1 , 0,
coordinates(j,1), coordinates(j,2), coordinates(j,3));
        end
        fclose(fid);
    end
end
length(unique(coordinates(:,1)))<size(coordinates,1)
```

```
scatter(coordinates(:,1),coordinates(:,2),'filled')
axis equal
axis off
```

APPENDIX A2: Lammps Input Script

```
variable struc loop 1 11

shell mkdir T$(v_struc)
shell cd T$(v_struc)

log T$(v_struc).60x60.1.${temperature}K.log

units       real
dimension   3
atom_style  charge
neighbor    0.3 bin
processors  14 2 2
timer       full sync
comm_style  tiled

boundary    p p p
read_data   ../../T$(v_struc).60x60.1.lammpsdata
mass        1 10.811

variable pressure equal 0
variable tstep equal 0.1 #for S1, S5 and S6 use 0.1
variable strainmax equal 0.3
variable srate equal 1e9/1e15
variable tmp equal bound(all,xmax)-bound(all,xmin)
variable lenx equal ${tmp}
variable vtension equal sqrt(${srate}*${srate})*${lenx}
variable nstep equal ${strainmax}*${lenx}/${vtension}/${tstep}
variable restart equal ${nstep}/4
variable dumpfreq equal ${nstep}/20

pair_style reax/c ../../lmp_control checkqeq no
pair_coeff * * ../../ffield.reax.CBN B

dump        1 all custom 100 dump.minimization id type x y z
fix         1 all box/relax x 0.0 y 0.0
min_style   cg
minimize    0.0 1.0e-6 100000 1000000
undump      1
unfix       1

compute     peratom all pe/atom
compute     speratom all stress/atom NULL
```

```
reset_timestep  0
timestep    ${tstep}
velocity    all create ${temperature} 12346 mom yes rot yes
balance    1.05 rcb

fix         1 all npt temp ${temperature} ${temperature} 20 iso
${pressure} 0 1000 drag 2
dump        1 all custom 1000
dump.T$(v_struc).60x60.1.${temperature}K.npt.optimize id type x y z
fx fy fz c_peratom c_speratom[1] c_speratom[2] c_speratom[3]
c_speratom[4] c_speratom[5] c_speratom[6]
fix         2 all reax/c/bonds 1000 bonds.reaxc.optimize
thermo      1000
thermo_style    custom step lx ly lz press pxx pyy pzz pe temp
neigh_modify    every 2 delay 10 check yes page 100000
run         10000
reset_timestep  0
unfix       1
unfix       2
undump      1

write_restart restart.T$(v_struc).60x60.1.${temperature}K.equil

variable    tmp equal lx
variable    lx0 equal ${tmp}

fix     1 all npt temp ${temperature} ${temperature} 20 y 0 0 1000
z 0 0 1000 drag 2
fix     2 all deform 1 x erate ${srate} units box remap x
fix     3 all reax/c/bonds 1000 bonds.reaxc.tension

variable    strain equal "(lx-v_lx0)/v_lx0"
variable    p1 equal v_strain
variable    p2 equal "-1.01325*0.0001*pxx*(ly*lz*0.01)"
variable    p3 equal "1.01325*0.0001*pyy"
variable    p4 equal "1.01325*0.0001*pzz"
variable    p5 equal lx
variable    p6 equal ly
variable    p7 equal lz
fix     def1 all print 1000
"${p1}   ${p2}   ${p3}   ${p4}   ${p5}   ${p6}   ${p7}" file
T$(v_struc).60x60.1.${temperature}K.strain.dat screen no
dump        1 all custom 1000
dump.T$(v_struc).60x60.1.${temperature}K.tension id type x y z fx
fy fz c_peratom c_speratom[1] c_speratom[2] c_speratom[3]
c_speratom[4] c_speratom[5] c_speratom[6]

thermo          1000
thermo_style    custom step temp v_p1 v_p2 v_p3 v_p4 ke pe press
```

```
run             ${nstep}    #nstep equal
${strainmax}*${lenx}/${vtension}/${tstep}

unfix 1
unfix 2
unfix 3
unfix def1
undump 1

shell cd ..
clear
next struc
jump B.tension.in
```

APPENDIX A3: Effect of strain rate and size

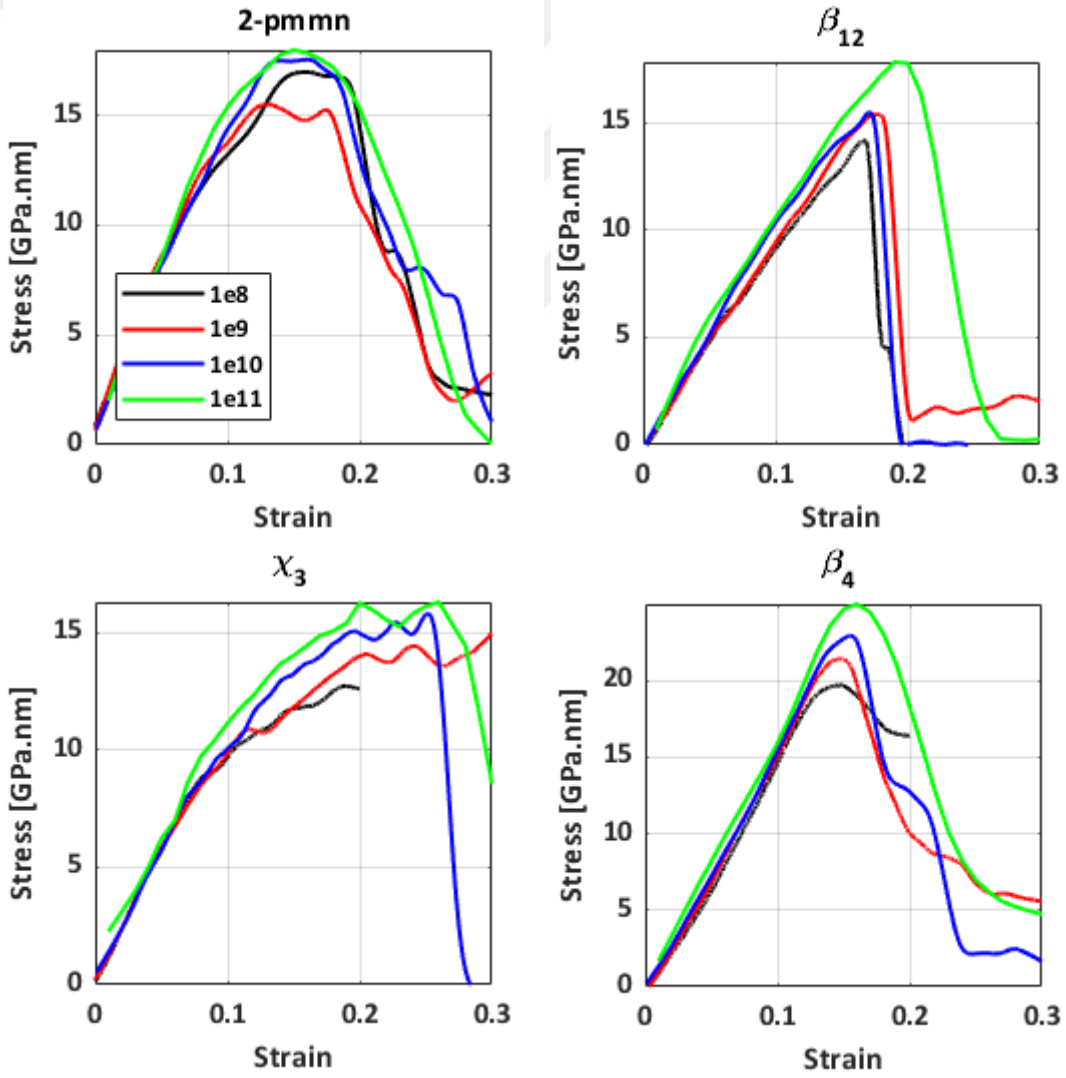

Figure A3.1: Different strain rate comparisons for zigzag structures.

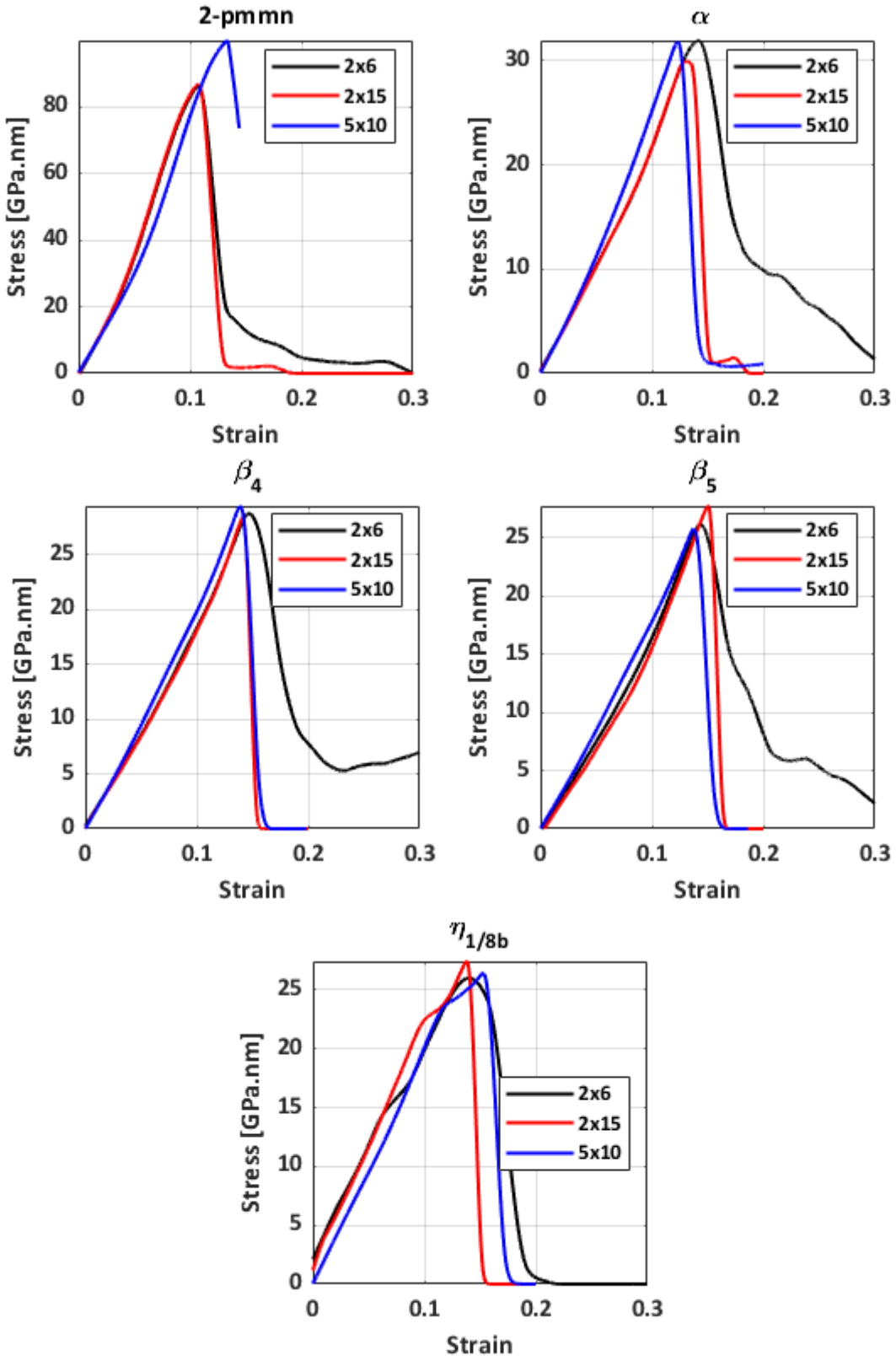

Figure A3.1: Different size comparisons for zigzag structures.

CURRICULUM VITAE

Name Surname : Erdem ÇALIŞKAN

EDUCATION :

- **B.Sc.:** 2020, Istanbul Technical University, Mechanical Engineering
- **M.Sc.:** 2021 (expected), Istanbul Technical University, Mechanical Engineering, Solid Mechanics

PROFESSIONAL EXPERIENCE AND REWARDS:

- 2020-2021: Structural Analysis Engineer, ITUNOVA Technologies

PUBLICATIONS, PRESENTATIONS AND PATENTS ON THE THESIS:

- **Çalışkan, E. and Kırca, M.** (2021). Mechanical Properties of Boron Nanotubes with Triangular Lattice, *6th International Erciyes Conference on Scientific Research*, 1-2 September, Kayseri, Turkey, pp. 349-351 , ISBN:978-625-7464-11-6